1296

University of Neuchâtel

Microfabricated Tools for the Scanning Force Microscope

A dissertation
submitted to the Faculty of Science of the University of Neuchâtel, in fulfillment of the requirements for the degree of "Docteur ès Sciences"

by

Jürgen Brugger

Dipl. électronique-physique
University of Neuchâtel, Switzerland

Institute of Microtechnology
Rue Jaquet-Droz 1, CH - 2000 Neuchâtel
Switzerland

1995

IMPRIMATUR POUR LA THÈSE

Microfabricated Tools for the Scanning Force Microscope

de M. Jürgen Brugger

UNIVERSITÉ DE NEUCHÂTEL

FACULTÉ DES SCIENCES

La Faculté des sciences de l'Université de Neuchâtel sur le rapport des membres du jury,

Messieurs N. de Rooij, P. Martinoli, U. Staufer (Bâle) et P. Vettiger (IBM Rüschlikon)

autorise l'impression de la présente thèse.

Neuchâtel, le 2 mai 1995

Le doyen:

H.-H. Nägeli

This Scanning Electron Micrograph shows the world's smallest and unfortunately unplayable bass-guitar. It is built by using micro-lithographic and etching techniques that were developed in this thesis for the micromechanical SFM device, just by changing the mask layout.

"I am surprised to see that you, who are such a tall person, can make things that are so tiny",
A Japanese friend at Hitachi Ltd., Tokyo, Summer 1994.

"N'hesitez jamais de poser des questions!"
Nico de Rooij in his lectures at the University Neuchatel.

Table of contents

Abstract

A scanning force microscope ressembles much to an old fashioned vinyl record player, where a needle is riding over the record grooves and picking up the music signal that is encoded in the topographical features. However, the pick up in a scanning force microscop is about 100 to 1000 times smaller. Hence, it can not be build with conventional fabrication techniques.

In a scanning force microscope a tiny cantilever beam with a sharp tip is used to image a sample surface with a resolution at the nanometer and even atomic scale. The requirements for the mechanical devices used in this application are very high, since they have to represent the interface between the millimeter and the nanometer world.

The fabrication of the tools is a typical application field for microsystem technologies. It borrows many process steps from the well established planar integrated circuit fabrication, and essentially extends them towards three dimensional micromachining in order to obtain the mechanical micro components and systems.

The results presented here summarize our exploration in this relatively new technology area for the development of miniaturized tools for the scanning probe systems. First it describes the silicon batch fabrication of nanometer sharp tips and micrometer sized cantilever beams. Then devices with an integrated electrostatic deflection sensor and actuator are introduced and used for non-contact mode imaging. Simultaneous parallel surface imaging with piezoresistive deflection sensors is shown, presenting a remedy to the inherent slow scan rate of single probes. And finally, a piezoresistive lateral force sensor is demonstrated for use in nano-tribological experiments.

This thesis is intended to contribute to the advancement of micromachining technologies in the area of local probe instruments. In particular it shall contribute to the cost effective fabrication of large amounts of micro-devices which are needed to satisfy the demand for silicon tools in the steadily growing market of surface scanning microscopes. Prospective applications also expant into the domain of proximal probe nano-lithography or high-resolution data storage.

Acknowledgments

First of all I would like to thank Nico de Rooij for his enthusiastic support in this fascinating project. It was a great honor and pleasure for me to work in his group at the IMT, where he has put together such a motivated and successful team of scientists and excellent technicians. I appreciated very much his fine guidance through the inevitable difficulties in the project realization, and his encouragement that we present our results to the outside of the institute. He allowed me to make mistakes and so I learned from them. I would also like to thank Nico that he encouraged and allowed me to spend one year at the Hitachi Lab in Tokyo for pursuing my research there.

I acknowledge Prof. P. Martinoli from the Physics Department, University of Neuchatel, Urs Staufer from the University of Basel, and Peter Vettiger from IBM Rüschlikon, for kindly agreeing to be examiners of my thesis.

Many thanks to our secretaries, Antoinette Goumaz-Rebetez and Margrit Ruegg who kept our hands free from bureaucratic load.

I wish to thank all my colleagues at the IMT for the long moments spent together in the microfab lab. Since my first hours in the cleanroom I always enjoyed the time doing the silicon micromachining processes. Often I felt myself like cooking a meal in a huge kitchen, with all the machines and tools and other cooks and chefs around. Here a little spin coating of a thin layer onto a wafer, baking it (just like a pizza) at 120 deg C for about half an hour; there an exposure to a reactive plasma for 10 minutes, adding here and there a drop of glycerin to hydrofluoric acid for better results. By using our standard recipes and trying exotic new ones we all found menus for unbelievable novel silicon microstructures.

I acknowledge in particular (with the risk to forget some names), Thomas Tschan for many helpful discussions on microfabrication processes and the finite element analysis of mechanical devices and for lending me his windsurfing board on the lake of Neuchatel. I thank Thomas and Christian Linder for the collaboration in the dry etching. Christian, during long night sessions, also proofread my reports and corrected (while I was sleeping at home) the scientific and spelling mistakes. I would like to thank Victor Jaecklin for the exchange of ideas concerning the xy-scanner and many other micromechanical issues. Also, I thank Ruedi Buser for the collaboration during the first phase of the project.

I would like to acknowledge Nicolas Blanc and Urs Duerig (IBM Ruschlikon) for the collaboration and the experiments with the capacitive cantilever.

I thank David Strike for his English humor in the shared office space, for lending me his favorite Jazz CD's, and for keeping the discussion, Apple versus PC, alive. Many thanks to Lionel Paratte for helping me to understand the differential equations of the mechanical behavior of cantilever beams.

I would like to thank Philippe Arquint for his kindness in helping me in any possible problem and for lending me his flat for a while, Cynthia Beuret for organizing Squash tournaments and ski weekends and Pierre-Francois Indermuhle for the collaboration with the microscanner device.

Many ideas originated (and apparent 'show stoppers' of a process flow often were eliminated) during coffee break discussions at the IMT, where 4 languages at least were spoken simultaneously, and I remember in particular Albert van den Berg, Bart van der Schoot, Appolonius van der Wiel, Peter van der Wal, Milena Koudelka-Hep, Florence Paoletti, Pierre Thiébaud, Georges Racine, Cornel Marxer, Philippe Luginbuhl, Jean-Charles Fiaccabrino, Marc Boillat, Marc Grétillat and Volker Gass.

Most of the work that I accomplished would not have been possible without the help of Sylviane Pochon, Sabina Jenny, Sylvain Jeanneret and Pierre-André Clerc, our excellent technicians who run the microfab lab.

I acknowledge the collaboration with many people from the Centre Suisse d'Electronique et de Microtechnique (CSEM S.A.), especially the staff from the mask making shop, Philippe Renaud for the discussion on capacitive sensors and Jean-Pierre Thiébaud from the microfab for helpful discussions on dry etching, and for introducing me to the Swiss Alpine Mountain Club. Rainer Christoph, Jürgen Burger (spelling ok!) and Martin Binggeli, alias Tinu, are acknowledged for the collaboration in many experiments, in particular for the tribological experiments, and even more for their friendship.

Gianni Mondin, Pierre Lacombe and Jean-Daniel Cretin from Microsens are acknowledged for their help in realizing some essential technological steps during the process and for their uncomplicated way of circumventing bureaucratic complications.

I thank Lukas Howald and Martin Ruetschi from the University of Basel, and Marc Jobin from the University of Geneva for performing SFM experiments with our microfabricated structures.

It was also a unique chance for me to spend one year of my Ph.D. time at the Central and Advanced Research Laboratory, Hitachi Ltd., in Kokubunji-shi near Tokyo, which is a fantastic research facility. I would not have enjoyed my stay in Japan as much as I did, if there had not been all the colleagues and friends.

First of all I am very indebted to Imura-san and his family and to the members of Group 306 at Hitachi ARL, namely Kanou-san, Hosaka-san, Kikukawa-san, Nakamura-san, Miyamoto-san, Koyanagi-san, Shintani-san and Etoh-kun for their extraordinary hospitality and helpfulness to overcome any imaginable Gaijin-trap I possibly could fall into. I would like to thank many other people that I met in Tokyo for their friendship, in particular Yuko Nakamura, Katsumi Yoneda, Shinya Akamine, Emi Watanabe, Fumiaki Hamazato, John Bonevich, Dave Donnet, Stefan Foelsch, Stefan Hoin and Akitoshi Toda. Financially my stay in Japan was supported by HIVIPS, the Hitachi Invited Visiting Research Program.

The Swiss National Science Foundation (NFP24 and NFP24+) is gratefully acknowledged for the financial support of a major part of this project.

I wish to thank very very much my family, both at home in Rheinfelden/Germany and in Neuchatel/Switzerland, for financial and moral support all over the years in so many circumstances, and for letting me go my way.

Merci beaucoup! Danke schön! Arigato o-gozaimasu!

List of figures

List of tables

1296

Chapter 1
The Scanning Force Microscope

1.1 Principles of a Scanning Force Microscope

The scanning probe microscope

In 1981 Gerd Binnig, Heini Rohrer and co-workers at the IBM Forschungslaboratorium in Rüschlikon presented surface images on the atomic scale by using the so-called Scanning Tunneling Microscope (STM)[1]. With this invention, they revolutionized the field of surface physics and related science and technology. In a STM, a tip is raster scanned within an extremely short distance across a sample surface, such that, when a bias voltage is applied between the tip and the sample, a tunneling current can be established. This tunneling current is an exponential function of the tip-sample distance and thus yields information of topographical and/or electronic properties of the surface with extremely high spatial resolution.

The tremendous success of the STM has triggered the development of an impressive family of Scanning Probe Microscopes (SPM), e.g. the Scanning Force Microscope (SFM), (or Atomic Force Microscope, AFM)[2], the Near-field Scanning Optical Microscope (NSOM)[3], the Magnetic Force Microscope (MFM)[4], and others[5,6].

All SPMs have basically one principle in common: they limit the interaction range between the probe tip of the microscope and the sample features to a tiny spatial spot to achieve the extremely high local resolution.

For today's industrial applications for surface inspection, the SFM is probably the most popular of all the SPMs. This is mostly due to its widespread range of applications: contact mode or non-contact mode imaging, on conducting or insulating materials, with flat of rough topographic features, for nano-metrology or surface indentation, etc.

The popularity of the SFM is a consequence of its relative ease in use and robustness for operation in daily circumstances, and thanks to the mass-fabricated force sensors which are readily available at relatively low cost and which match the needs of the specific applications.

In the future the NSOM might challenge the SFMs first place, because it allows high resolution optical imaging beyond the diffraction limit while maintaining compatibility with many techniques used in conventional optical microscopy. However, this will not happen prior to the development of suitable, reproducible and inexpensive optical probes.

With all the differences in surface imaging modes and capabilities of the various types of SPMs, they should be considered to be rather complementary than competitive to each other.

The scanning force microscope

The SFM was developed in 1986 by Gerd Binnig, Cal Quate and Christoph Gerber at Stanford University[2]. Instead of measuring a current, as it is done in the STM, the SFM uses a mechanical transducer to measure small forces between a sharp tip and the sample surface. It extends the range of specimen to insulating materials, which cannot be imaged with the STM. To achieve the extremely high resolution, the SFM uses a probe that consists of a tiny single side clamped cantilever beam with a tip at the free end, which is riding on (or closely over) the surface. In the presence of surface protrusions or forces acting between the surface and the tip, the cantilever follows the surface topography (or the equi-force contour line respectively) by a bending motion. This principle has already been exploited by profilometers for many years. New in the SFM is that, by using a feedback system, the contact pressure between the tip and the sample can be controlled and adjusted very accurately, in order to become more sensitive to the various forces, and hence to raster scan with extremely small contact pressure over the specimen.

The principle of an SFM and a typical set-up of the instrument are shown in Fig. 1.1. The following list denotes the components that are essential for a SFM:

A a *sharp tip* which is important for high lateral resolution

B the *spring* in the shape of a cantilever, that transmits (by Hook's law) the force interaction of the tip into a controlled mechanical cantilever deflection

C the *sensor*, for measuring the deflection of the cantilever

D the *actuator*, for moving the tip with respect to the sample (or vice versa) in a controlled xy-direction, and for the feedback in z-direction

E the *computer*, for controlling the system and for acquiring and visualizing the data

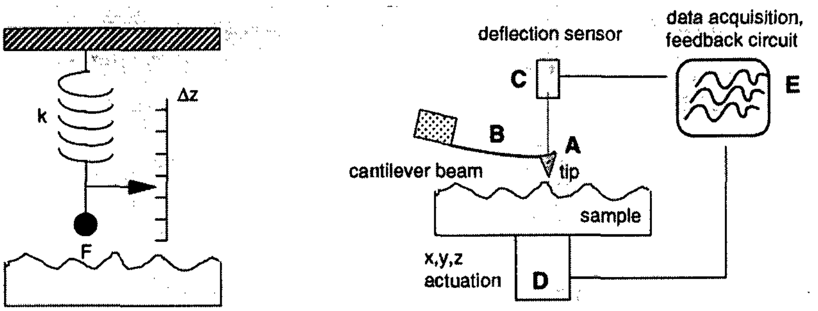

Fig. 1.1: Principle of a scanning force microscope (left) and bloc diagram of its essential parts (right).

According to the literature, the first SFM used an assembled set-up: the spring like cantilever was a sharpened metal wire or a cut aluminum foil whose edge, or later eventually a glued diamond fragment, served as the tip; the cantilever motion was monitored by a tunneling tip; and finally the raster scan and feedback actuation mechanism was the tube scanner made of piezoelectric zirconium titanate (PZT). Astonishingly, with such 'hand-crafted' set-up's atomic scale images could be achieved on flat/layered samples[2].

However, a major drawback was soon identified: those tips and cantilevers were not reproducible. As a consequence the mechanics of the transducer was not well known, such that a standardization of the measurement was impossible. The first reproducible force sensors of thin film silicon dioxide or nitride with a well known geometry and with integrated tips were microfabricated by Albrecht and coworkers[7] at Stanford University in 1990. Later, silicon cantilevers were introduced by Wolter and coworkers[8] at IBM Sindelfingen. These cantilever probes are mass fabricated and distributed by several companies.

D the *actuator*, for moving the tip with respect to the sample (or vice versa) in a controlled xy-direction, and for the feedback in z-direction

E the *computer*, for controlling the system and for acquiring and visualizing the data

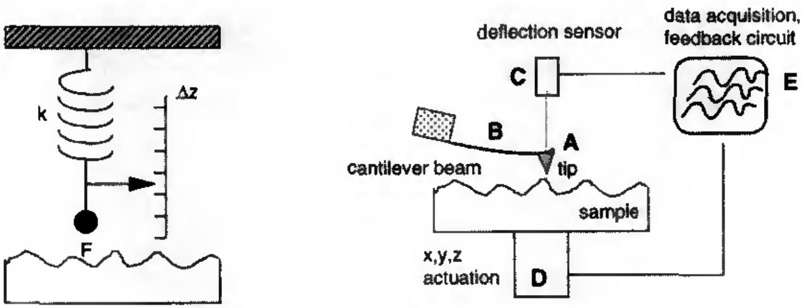

Fig. 1.1: Principle of a scanning force microscope (left) and bloc diagram of its essential parts (right).

According to the literature, the first SFM used an assembled set-up: the spring like cantilever was a sharpened metal wire or a cut aluminum foil whose edge, or later eventually a glued diamond fragment, served as the tip; the cantilever motion was monitored by a tunneling tip; and finally the raster scan and feedback actuation mechanism was the tube scanner made of piezoelectric zirconium titanate (PZT). Astonishingly, with such 'hand-crafted' set-up's atomic scale images could be achieved on flat/layered samples[2].

However, a major drawback was soon identified: those tips and cantilevers were not reproducible. As a consequence the mechanics of the transducer was not well known, such that a standardization of the measurement was impossible. The first reproducible force sensors of thin film silicon dioxide or nitride with a well known geometry and with integrated tips were microfabricated by Albrecht and coworkers[7] at Stanford University in 1990. Later, silicon cantilevers were introduced by Wolter and coworkers[8] at IBM Sindelfingen. These cantilever probes are mass fabricated and distributed by several companies.

A further simplification for the SFM operation stems from a new cantilever deflection method that uses an optical beam detection[9]. This method is highly accurate and is considerably easier to use than the tunneling technique. The main reason for this is that the working distance between the detector and the cantilever lies in the range of several mm, instead of a few nm, as previously.

Further advances in scanning force microscopy were triggered by the development of various other cantilever deflection methods: interferometer[10,11,12], capacitive[13,14], and piezoresistive[15]. Each method has its own advantages and drawbacks, and is more or less suited for the individual mode of operations of the SFM. An overview of the different methods with their characteristics is presented in Table 1.1 at the end of this chapter.

Miniaturization of the SFM

Fig. 1.2: Chip with silicon cantilever and tip held by tweezers. The picture demonstrates how a series of transducers are used to bridge the gap of 9 orders of magnitude between the human dimensions (10^0 m) to the nanometer scale world (10^{-9} m).

The SFM serves as a transducer to bridge the gap of 9 orders of magnitude between our world (10^0 m) down to the 'nanoworld' on the 10^{-9} m scale and below. The primary stage of the transducer is the probe consisting of the tip (nm -> µm). The next stage is the cantilever (µm -> mm). The third stage is the handling piece to which the probe is attached (mm -> cm) so that we can hold it in our hand, and also the detector and scan actuator.

It has been recognized early that by decreasing these dimensions and by bringing more functionality down to the probe an improved performance can be achieved. In particular mechanical noise is a major concern and it is well known that the immunity against vibration and thermal noise increases with decreasing size.

The use of micron sized cantilevers is *the* proof for this: SFM cantilevers have typically spring constants in the range of 1 N/m, so that a small force of, say 10^{-9} N, deflects the spring by 1 nm, which lies in the range of most detectors. A simple example demonstrates the necessity of size reduction of the SFM components: a silicon cantilever with a length of 300 μm, a width of 40 μm and a thickness of 3 μm, has a spring constant of about 1.7 N/m. A spring constant in the same order of magnitude can be obtained by a rectangular plate of copper having a length of 30 cm, a width of 1 cm and a thickness of 0.5 mm. The resonance frequencies however for the macro sized cantilever lies in the order of 3 Hz, for the micron sized cantilever at about 45'000 Hz! Due to this high resonance frequency it is less effected by environmental vibration noise than its macroscopic counterparts, and has a short response time on fast mechanical perturbations, and is thus able to follow rapidly changing surface variations, which is indispensable for a high imaging speed.

Logically, the next step to decrease the size of an SFM system is to replace the external sensor and actuator parts and to integrate these functions into the probe itself. This trend has been set in 1989 by Akamine and coworkers[16] who developed a three dimensional actuated cantilever made by piezoelectric materials, and in 1991 by Tortonese and coworkers[15] who developed an integrated silicon cantilever with a piezoresistive deflection sensor. Probes with integrated functions give access to parallel surface imaging by using an array of tips with a tremendous increase in scan rate compared to the slow operation of a single probe.

1.2 Force transducers for SFM: design and mechanics

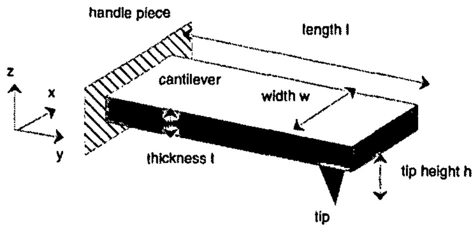

Fig. 1.3: Annotation of the dimensions for the single side clamped cantilever with rectangular cross section as used in the analysis.

The force sensor is the central component of an SFM and it has to fulfill specific requirements. It should be flexible in one direction, but stiff in all others. It should have a sharp tip integrated at the front part of the lever for local surface contacts. For easy sample access it should protrude away from a piece that is big enough for handling purposes. It should match the required mechanical characteristics (spring constant, resonance frequency). And it should be reliable, easily replaceable and cheap.

The requirements for the mechanics can be best fulfilled by using a single side clamped cantilever beam of rectangular shape (Fig. 1.3). For increased lateral stiffness a triangular shape might be preferable. The spring constant k of such a cantilever with constant cross section is $k = 3\,E\,I / l^3$. E denotes the modulus of elasticity (or Young's modulus) of the material and I denotes the cross sectional moment of inertia. For a rectangular shaped cross section $I = wt^3/12$ and we obtain[17]

$$k = \frac{E\,w\,t^3}{4\,l^3}\ . \tag{1.1}$$

The cantilever beam can be vibrated by a mechanical, acoustical or thermal excitation. The first resonant frequency f is given by

$$f = \frac{1}{2\pi}\sqrt{\frac{k}{m_{eff}}}\ , \tag{1.2}$$

where m_{eff} is the effective mass of the lever which is given be $m_{eff} = m_c + 0.24\ m_d$. Here, $m_d = l\ w\ t\ \rho$ is the distributed mass of the lever, with ρ the density of mass, and m_c is the concentrated mass of the tip[18]. Since for typical probes m_c is considerably smaller than m_d we will neglect it in our analysis, and we set $m_{eff} = 0.24\ m_d$.

For typical SFM applications the levers should have a spring constant between 0.01 and 100 N/m and a resonance frequency above 10 kHz. Equation (1.2) shows again that the simultaneous matching of a high resonant frequency f with a low spring constant k can only be obtained by a miniaturized device with a small mass.

Thermally induced noise Δz of a free standing cantilever of spring constant k at the absolute temperature T is given by

$$\Delta z = \sqrt{\frac{k_B T}{k}}, \tag{1.3}$$

where $k_B = 1.38 \times 10^{-23}$ J/K is the Boltzmann constant. For a freestanding cantilever with k = 1 N/m at room temperature the amplitude of noise vibration amounts to about 0.6 Å. When the tip is in contact with the sample (contact mode) then this degree of freedom vanishes.

1.3 Measurement of cantilever deflection

We will briefly describe the various configurations that have been implemented to measures the minute force-induced deflections of the flexible lever supporting the force-sensing tip. A summary is given in Table 1.1. at the end of this chapter.

Tunneling detection system[1]

A fine conducting tip is approached to a few nanometers to the (metallized) backside of the cantilever. When biasing the tip and the lever, a tunneling current can be established. The tunneling current density is exponential in the tunneling gap which makes this method *extremely sensitive*. As a consequence of the close proximity of the sensor tip however, the cantilever deflection is very limited, unless it is operated with a feedback in a constant force regime. The sensing interaction is between a single atom at the apex of the tip and its closest atom on the lever such that a lateral motion of the cantilever can influence the signal. Other drawbacks are the strong attracting forces occurring between the tip and the cantilever, and also the contamination films on the lever, which can lead to instabilities. The tunneling technique is best suited for ultra-high vacuum environments.

Beam deflection system[9]

This is today's most utilized method. A collimated laser beam is focused on the cantilever and is reflected back into a two-segment photo detector. A minute deflection of the lever causes one detector segment to collect more light than the other. The signal is fed into a differential amplifier representing the measured displacements, i.e. forces. The operation of this technique is *very simple and accurate*. A great advantage is that the detector is placed at a large distance of the probe. When using a four-segment detector, then also the torsion of the lever can be monitored. This scheme finds application in tribology or friction microscopy.

Fiber interferometer system[10,11,12]

An optical glass fiber is approached within a few μm to the back of the lever. The coherent light of a laser diode coming through the fiber is reflected both on the lever back and internally at the glass-air interface of the fiber. The interference of the re-entering light is used to detect the motion of the cantilever. An advantage here is that the wavelength of the laser light can be used as an *absolute standard*.

Capacitive system[13,14]

A rigid reference electrode is approached to a few micrometers to the back side of cantilever. The capacitance between the lever and this electrode is a function of the gap in between. The drawback of this method is that very small changes of capacitance have to be measured, which requires rigorous electrical shielding of device against parasitic capacitance. On the other hand, by means of electrostatic forces, the cantilever can be *actuated* and the *force constant can be modulated.* This makes the capacitive system to a predestined method for *dynamic mode force microscopy.* By using microfabrication techniques it is possible to build closely spaced electrodes with a precise gap. Capacitive sensors can thus be made very compact. It is also possible to build multiple probe arrays with this technique. We will discuss this system in detail in chapter 3.

Piezoresistive system[15]

This technique exploits the so-called strain-gauge principle. The resistivity of silicon changes when stress or strain is applied to the crystal. By integrating resistor loops directly into the lever, the resistance change can be measured with a bridge set-up. Since the detector is directly incorporated in the lever itself, this system is the *most compact* of all detection systems. No external assembling is required. It is also a candidate for parallel tip array operation. A drawback of the piezoresistive system is the strong influence of temperature effects, therefore compensating structures should be included in the device. A piezoresistive device will be discussed in chapter 4.

Table 1.1 The various methods to detect the deflection of the cantilever in a scanning force microscope

Detection method	detector distance	µ-fabrication feasible ?	advantages	drawbacks	reference
Tunneling 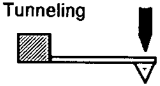	≅ 1 nm	yes	high resolution	positioning; close to probe; contamination	1
Beam deflection 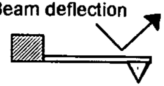	5 - 50 mm	no	very simple	noise of laser diode limits the DC resolution	9
Interferometer 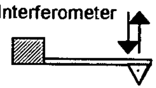	a few µm	no	wave length as absolute standard; very stable	positioning difficult	10,11,12
Capacitance 	a few µm	yes	force constant modulation by electrostatic field	damping, critical operation	13,14
Piezoresistor 	none	yes	very compact	temperature dependence	15

[1] G. Binnig, H. Rohrer, Ch. Gerber and E. Weibel, Phys. Rev. Lett. 49, 1982, p. 57

[2] G. Binnig, C.F. Quate and Ch. Gerber, Phys. Rev. Lett. 56, 1986, p. 930

[3] D.W. Pohl, W. Denk, M. Lanz; Appl. Phys. Lett. 44, 651 (1984)

[4] U. Hartmann; J. Appl. Phys. 64, 1561 (1988)

[5] 'Scanning Tunneling Microscopy and related techniques', R. Wiesendanger, H.J. Güntherodt (eds), Springer Berlin, 1992

[6] 'Scanning Probe Microscopes'; K. Wickramasinghe, Scientific american (October 1989)

[7] T. Albrecht, S. Akamine, T.E.Carver, C.F. Quate, J. Vac. Sci. Technol. A8, 1990, p. 3386

[8] O. Wolter, Th. Bayer, J. Greschner, J. Vac. Sci. Technol. B9, 1991, p. 1353

[9] G. Meyer, N.M. Amer, Appl. Phys. Lett. 53, 2400 (1988)

[10] D. Rugar, H.J. Mamin, R. Erlandsson, J.E. Stern, B.D. Terris, Rev. Sci. Instrum. 59, 2337 (1988)

[11] C. Schönenberger, S.F. Alvarado, Rev. Sci. Instrum. 60, 3131 (1989)

[12] D. Anselmetti, Ch. Gerber, B. Michel, H.-J. Güntherodt, H. Rohrer, Rev. Sci. Instrum. 61, 3003 (1992)

[13] T. Göddenhenrich, H. Lemke. U. Hartmann, C. Heiden, J. Vac. Sci.Technol. A8, 383 (1990)

[14] G. Neubauer, S.R. Cohen, G.M. McClelland, D. Horne, C.M. Mate, Rev. Sci. Instrum. 61, 2296 (1990)

[15] M. Tortonese, R.C. Barrett, C.F. Quate, Appl. Phys. Lett. 62, 834 (1993)

[16] S. Akamine, T. Albrecht, M. Zdeblick, C.F. Quate, Sensors and Actuators A, 21-23, 964 (1990)

[17] I. Szabo "Einführung in die Technische Mechanik", Springer Verlag, Berlin (1954)

[18] D. Sarid, Scanning Force Microscopy, Oxford University Press, New York, Oxford, 1991

1296

Chapter 2

Microfabricated tips and cantilevers for the scanning force microscope

Several fundamental different methods for producing tips on cantilevers for the SFM exist and have been presented. Not all of them are compatible with IC fabrication techniques or suitable for mass fabrication. Tips can be made either by deposition techniques or by etching techniques, as summarized in Table 2.1. The first category includes the deposition of a sputtered material, e.g. aluminum, through a shadow mask which builds up a tip like metal column[1], and focused e-beam assisted deposition of a contamination shaft inside a SEM[2]. The second method includes the etching of silicon to form the tip[3] and to some extend focused ion beam milling (FIB)[4]. Another method involves the etching of a molding groove prior to the deposition, patterning and releasing of a structure material that incorporates the tip, e.g. silicon nitride[5].

Some of these methods produce very sharp and high aspect ratio tips (e-beam and FIB technique) but unfortunately they rely on the use of complex manufacturing equipment and lack in compatibility to a batch fabrication process.

The nitride levers developed at Stanford University are fabricated by anisotropically etching an inverted pyramid into the silicon by using KOH. Subsequent deposition and patterning of a low stress nitride layer and removal of the silicon bulk yields the nitride cantilever with nitride tips. This process is very simple and reliable since the etching of the pyramidal grooves is self terminated and sharpened due to the natural etch stop mechanism of

KOH at <111> silicon crystal planes and thus reproduces the tips very well. Cantilever with such tips are very popular and are fabricated and commercialized in high volume by several companies.

By using a silicon substrate with a tilt crystal angle tips having oblique pyramidal shapes could be produced. This would overcome the inherent problem of the undesired angle between the tip and the sample in SFM applications. Also, with the same molding technique tips with shapes other than a pyramid can be made. Olympus Opt. Co. has produced pencil shaped tips with high aspect ratios by using a deep RIE trench etching instead of KOH[6]. By using an oxidation sharpening technique the apex radius of the tips can be reduced further[7].

However, the nitride levers fabricated with the etch mold technique have one major drawback. The tip is on the 'wrong' side of the cantilever and points towards the side of the thick carrier chip where the tip can not access a sample surface. Therefore the wafer has to be bonded to a glass plate prior to the back etching and chip separation. A remedy to this has been shown by Akamine and co-workers who constructed a nitride cantilever with a tetrahedral silicon tip on the accessible side[8]. Nitride can be deposited and patterned with extremely high precision and consequently the spring constant and resonance frequencies of the levers can be predicted very accurately.

Silicon cantilevers and tips have been developed by Wolter and co-workers at IBM[9] and by ourselves[10]. The following paragraphs describe the fabrication process for tips, cantilevers and include a discussion on the feasibility of an array of parallel probes. Then imaging results are presented.

Table 2.1 *Overview of microfabricated SFM tips*

Fabrication technique	tip material	tip shape	aspect ratio	apex radius	batch compatible	ref.
deposition						
shadow mask	metal	conical	2:1	50 nm	yes	1
focused e-beam	organic composites	shaft	90:1	10 nm	no	2
milling						
focused ion beam	SiO_2 or any	arbitrary	-	-	no	4
etching						
+ molding	Si_3N_4	pyramid	1:1	30 nm	yes	1
		pencil	4:1	30 nm	yes	6
+ sharpened molding	Si_3N_4			~ 1 nm	yes	7
dry etching	Si	conical	~ 10:1	40 nm	yes	9,10
wet etching (isotropic)	Si	conical	2:1	50 nm	yes	11
wet etching (anisotropic)	Si	pyramid	1:1	15 nm	yes	11
sharpened etching	Si			< 1 nm	yes	13

2.1 Silicon tips

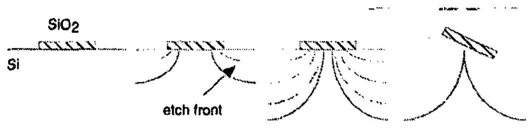

Fig. 2.1: Illustration of tip formation with silicon etch process

Silicon tip fabrication relies on the principle of the lateral under etching of a circular or polygonal mask layer. Wet anisotropic, wet isotropic and dry etching techniques can be used. Wet anisotropic etching, using the KOH etch solution with specific concentrations, exploits the difference in etch rates of higher indexed silicon crystal planes (e.g. <211>) to obtain highly protruding tips with steep side walls[11]. A dry etching process is also suitable to undercut a small etch mask to form a tip which is a fully IC process compatible method and thus allows for a very flexible process flow design. The ratio of undercut and etch depth can be determined by the etch parameters.

For our purpose of tip fabrication we developed a dry and wet etching process. First we pattern a silicon dioxide mask to a circle or polygon with a diameter of about 10 to 15 μm at the desired location of the future tip. By means of RIE this pattern is transferred into the silicon whereby the side wall shape of the appearing undercut as well as the etch depth, and with this the tip height, can be defined quiet accurately by the etch parameters, which is a major advantage of this technique. Typically we us a gas mixture containing SF_6 and C_2ClF_5. A schematic illustration of the tip formation process is shown in Fig. 2.1. The etching is finished when the tip mask is completely undercut and falls off. A tip height of up to 20 μm could be achieved by this method. With this technique we can fabricate silicon tips with radii as small as 30 nm.

Fig. 2.2 shows some SEM micro graphs of silicon tips with different shapes obtained with the described methods. A precisely timed process is necessary in order to avoid the over etching of the tips as no suitable etch stop mechanism exists. In the case of over etching the tip would round off and would decrease in height.

The lack of an efficient etch stop represents the major drawback of this kind of tip fabrication. The high compatibility to various other processes and its flexibility however makes it very interesting to be considered as part of a more complex device fabrication sequence. Furthermore, special tip shapes can be achieved as shown also in Fig. 2.2 (lower right). Such a tip can be useful for the imaging of the side walls of steep and narrow structures such as high aspect ratio photo resist patterns[12].

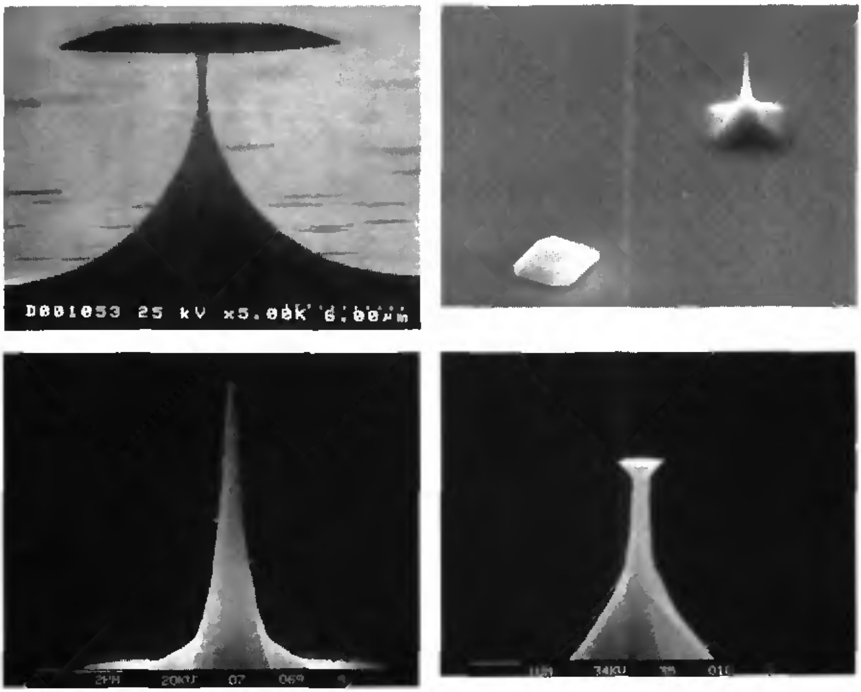

Fig. 2.2: SEM micro graphs of silicon tips with various shapes fabricated by etching techniques; with oxide cap when the etch is nearly completed (upper left), shortly after the etch is completed (upper right), high aspect ratio tip (lower left) and special tip for side wall imaging (lower right)

Low temperature oxidation sharpening

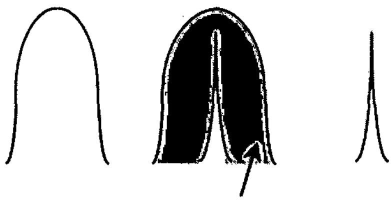

Fig. 2.3: Low temperature oxidation silicon tip sharpening technique; by anomalous oxide growth a silicon tip can be sharpened to a radius below 1 nm[13].

A nice method for obtaining ultra sharp silicon tips is the low temperature oxidation sharpening method. This technique exploits an anomalous oxide growth due to volume expansion which occurs at regions with high curvature radii[13]. It is *the* fundamental step to achieve ultra-sharp silicon tips. It can be used for the sharpening of already finished (and probably round off) tips as well as to the thin silicon shaft (as in figure 2.2 upper left). We illustrate this in Fig. 2.3.

The following experiment has been carried out at the Central Research Laboratory, HITACHI Ltd. We applied the sharpening technique to the silicon shaft directly after the dry etching process, when the shaft has an approximated width of about 0.5 µm. The oxidation duration is about Å 30 h, the temperature is set at 950_C resulting in a grow of about 433 nm of thermal silicon dioxide. For an easier sample preparation, we prepared test structures, consisting of parallel stripes with the same lateral pitch and width as used for the tips. After the thinning of the sample by an ion beam milling step, the structure was observed by a transmission electron microscope (TEM). Fig. 2.4 shows a high resolution image (x 4'000'000) of the tip apex. The interfaces between the grown amorphous silicon dioxide, the native oxide and the single crystalline silicon are clearly visible. The crystal lattice of silicon has a period of 3.2 Å. The tip which is still embedded in the dioxide has a radius of approximately 1.5 nm. Final removal of the dioxide in a BHF solution releases the tip.

The oxidation sharpening step is in general fully compatible with the overall processes that we use for the fabrication of the simple cantilever probes, the capacitive micro lever or the piezoresistive force sensor. Often the tip is etched at the beginning of the process and is then oxidized immediately. Hence it is protected inside the oxide embedding until the very end of the remaining process steps, when a final BHF etch step releases the silicon tip.

Fig. 2.4: High resolution transmission electron microscope image of the oxidation sharpened silicon tip. The tip is still embedded in the thermally grown dioxide. Magnification is 4 million. Image it taken by Mr. Kouguchi, Central Research Laboratory, HITACHI Ltd.

2.2 Silicon cantilevers with tips

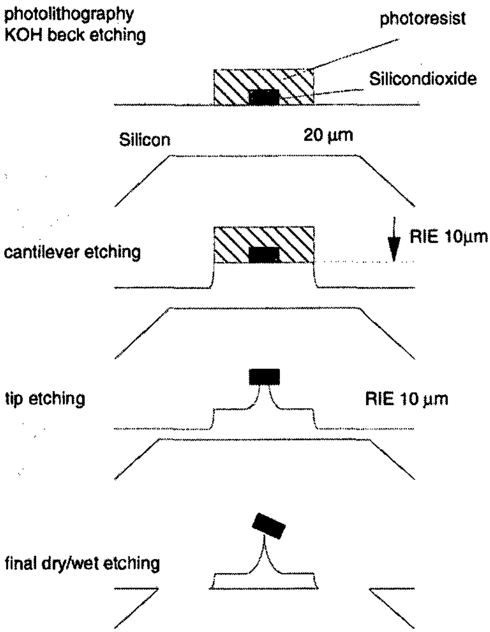

Fig. 2.5: Illustration of microfabrication process for silicon cantilever with silicon tips

One of the most intriguing challenges in a silicon microfabrication process for SFM microprobes is the integration of a sharp protruding tip onto a tiny flexible cantilever. For our purpose we developed an all silicon process using a combination of wet and dry etching steps. A first dry etching step is used to sculpture the cantilever and a second step for the tip. In our case, the mask used for the tip etching is patterned in silicon dioxide before the cantilever mask is deposited and structured. The oxide cap remains hidden under this mask layer until after the cantilever etching and resist stripping. The process is outlined in Fig. 2.5 and is described in detail hereafter.

A double side polished 280 μm thick (100) silicon substrate is used for our process. Their surfaces are thermally oxidized to 1.5 μm. On the topside the silicon dioxide is patterned to a tip mask of ~ 15 μm in diameter. Then a thick photo resist layer (~ 8 μm) is deposited and patterned to the cantilever shape. On the backside of the wafer, etch windows with compensation structures are opened in the dioxide for the wafer back etching. The anisotropic etch solution KOH (40 weight % @ 60_C, etch rate Å 17 μm/h) which etches preferentially the <100> silicon crystal plane and nearly stops at the <111> plane is used to fabricate a membrane of 20 μm thickness from the wafer back side. During this step the front side of the wafer is protected in a mechanical chuck using an O-ring seal. Since we do not use any etch stop mechanism in this process the etch depth is monitored with a precision point profiler instrument and the etching is accordingly timed to stop at the desired thickness. The precision of this technique allows the control of the membrane thickness within about 2 μm.

The top side is then dry etched using a chlorine/fluorine gas mixture to pre-shape the cantilevers to their desired thickness (typically 5 - 15 μm). The etch mask consist of thick photo resist. Due to re-deposition and surface passivation effects during this step good control of the side walls slope can be achieved[14]. The resist is stripped so that the oxide tip mask reappears. The tip etching is subsequently performed according to the previous paragraph. Simple dry etching or a combination of dry and wet etching can be used again. Silicon dioxide withstands well a succession of three or more etch steps. Fig. 2.6 shows SEM picture of finished devices with different cantilever thickness and tip shape.

The geometrical dimensions of the cantilever such as length and width are defined by the photolithography whereas the cantilever thickness is determined by both the backside KOH membrane etching and the top side RIE etching. Thus on one wafer batch the thickness of the cantilevers is the same whereas the length and width can be varied. We designed cantilevers with different geometrical sizes varying from lengths of 200 to 1000 μm and widths from 30 to 80 μm in order to obtain various mechanical characteristics for the different applications in mind. The cantilever thickness can be varied in a range of about 3 to 20 μm. It is obvious that the lack of a suitable etch stop mechanism is a drawback of this technique. However, fine adjustment of the process parameters allow for a high yield process with thickness variations of less than 1 μm from wafer to wafer. By using silicon-on-insulator (SOI) substrates a precise membrane can be achieved and thus the cantilever thickness predicted very accurately. Unfortunately SOl substrates are about ten times more costly and are therefore less suited for cost effective mass fabrication.

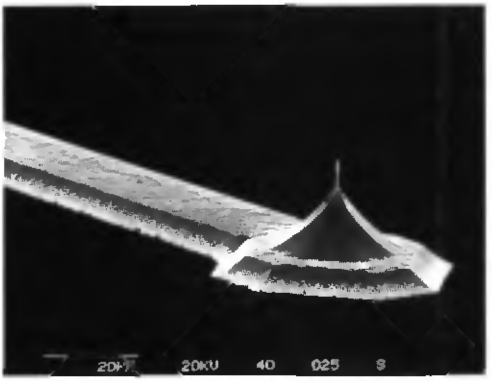

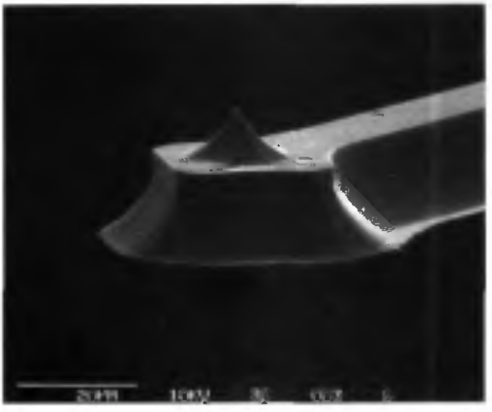

Fig. 2.6: SEM micro graphs of two microfabricated silicon cantilevers; the devices are stemming from different batches, therefore the thickness can vary from 5 µm to up to 20 µm; the tip shape can be varied with the etching parameters

2.3 Multiple probe array

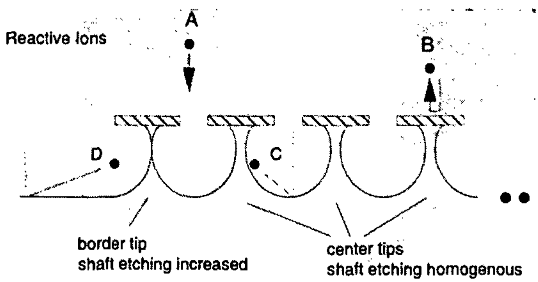

Fig. 2.7: Illustration of the etching behavior and tip formation in an array. The reactive ion A hits the surface and etches vertically, B bounces back from the tip etch mask. When the etching is continued C and D induce undercut of the mask. The lateral etch rate at a border tip is higher than for a center tip.

The probing of a surface using a single tip is a serial process and is therefore inherently slow. The use of an array of tips is one and probably the most promising remedy to this limitation. Hundreds, thousands or more parallel sensors could probe the surface with a hundred-fold, thousand-fold or higher scan rate. This issue becomes particularly important for industrial applications, for instance for the high resolution surface inspection of wafers in IC fabrication lines. Other potential applications for multiple probes are nanolithography where first experiments have been presented very recently[15] and ultra-high density data storage.

The fabrication of parallel micro cantilevers is as simple as the fabrication of a single tip - it is in principle only a question of the mask design. However, the etching of an array of tips exhibits some irregularities in terms of the reproducibility of their structural shape.

In order to investigate parallel tip fabrication at HITACHI we have prepared two dimensional test patterns of about 10 x 10 circular mask caps of 15 µm diameter silicon dioxide caps. We have designed various pitch distances to study the proximity effect during the etch process. The tips have been processed using a SF_6/O_2 gas. Fig. 2.7 illustrates the scheme of the etching. The etch ions arriving from the source in the plasma reactor chamber hit vertically into the substrate and etch into the silicon bulk. A fraction of the ions will bounce back randomly. Among other side etch effects due to the chemical etching these ions result in a lateral undercut of the tip mask (this is the major physical mechanism of the tip etching)[16].

The undercut rate is a function of the direct neighborhood conditions of each tip. For a tip that is surrounded by other tips the under-etching is homogenous. However, a tip at the border of the array is subject of an increased lateral etch rate due to the less masked neighborhood. This results in a narrower tip shaft. This result is shown in Fig. 2.8. It shows a close-up SEM micrograph of the corner region of the array (above), exhibiting well the difference in tip shape. Fig. 2.8 (below) shows the center of the same array with perfectly identical tips. For obtaining a highly homogenous tip array the lack of a suitable etch stop mechanism is clearly a drawback. A remedy to this could be to arrange dummy tips around the 'working' tips.

We also fabricated arrays of parallel cantilevers. Fig. 2.9 shows a SEM micro graph of four parallel cantilevers. The number of parallel probes can be defined by the mask layout. We have fabricated arrays containing up to 10 cantilevers. When designing a tip to tip distance of about 100 µm this is the maximum number of parallel probes for the typical cantilever holder that we were using (1 mm in width). The number of parallel probes in a two-dimensional array will ultimately be limited by the tip to tip distance, by the width of the cantilever, and also by the chip size. When using ultra-fine cantilevers[17] having a width of only 5 µm, a tip to tip pitch of roughly 10 µm might become feasible. With this arrangement 1000 probes could be placed laterally on the side of a 10 mm chip.

When using parallel surface probing, then each tip has to be addressable, for the cantilever motion monitoring (force) by using integrated deflection sensors, and for tip actuation (feedback). The latter is important when rough samples are investigated and the fly height of each individual tip over the sample must be adjusted. The important issue of actuated and sensed probes will be discussed in the following chapters.

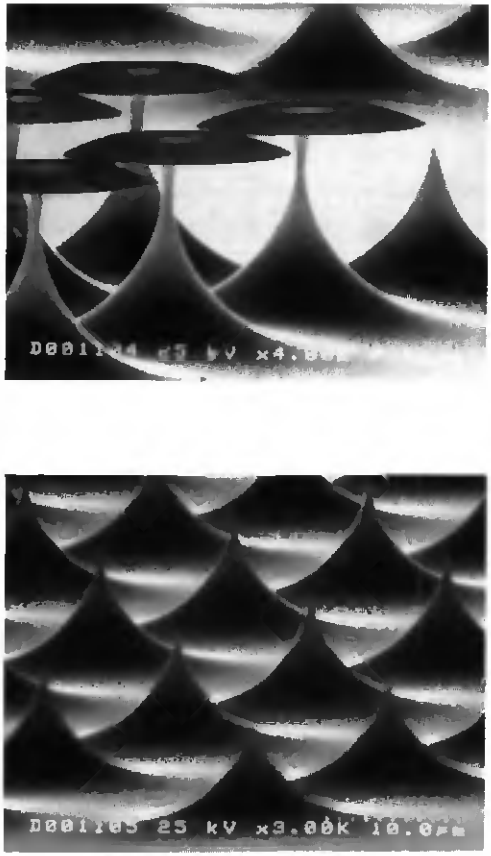

Fig. 2.8: SEM micro graphs of microfabricated silicon tip array. Corner region showing irregular tip shape due to a non homogenous under etch rate for border tips (above), center region with perfectly identical tip shapes (below)

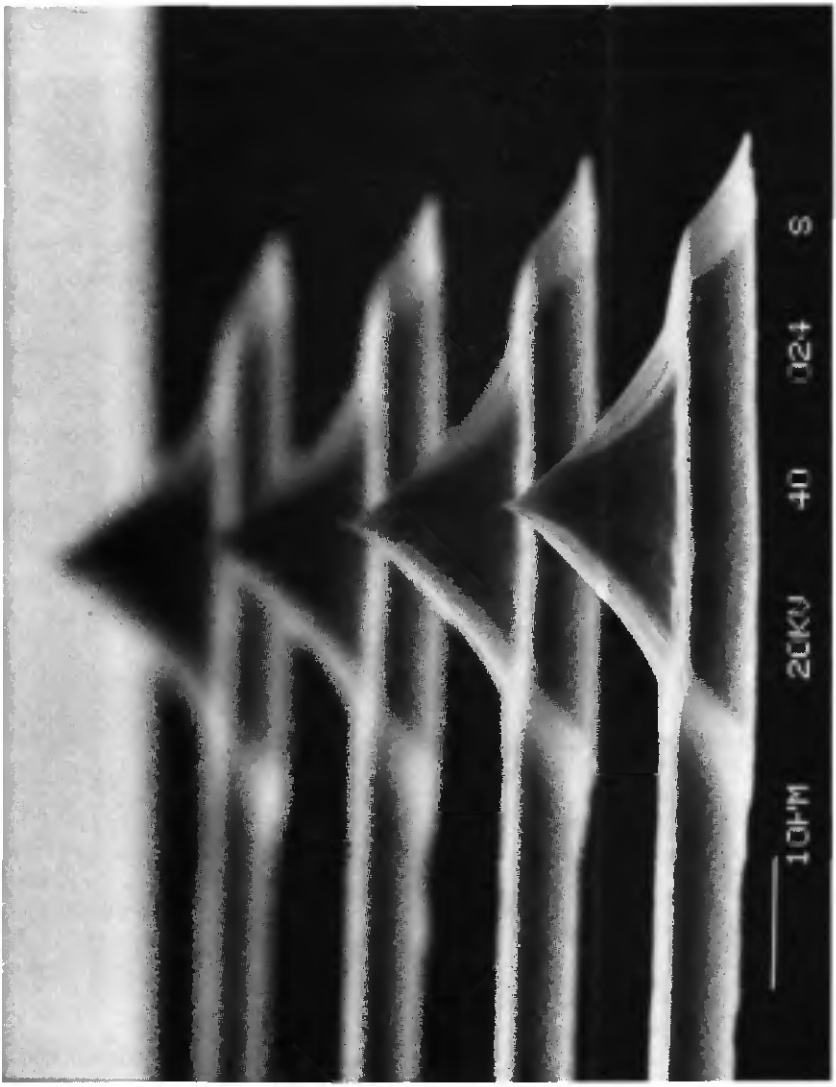

Fig. 2.9: SEM micro graph of an array of 4 microfabricated parallel silicon cantilevers with tips.

2.4 Surface imaging

Contact mode imaging

This is the mode of operation where the tip is in physical contact with the sample and is riding over the specimen surface topography. This is also the mode of operation that is used in nano-metrology applications[18], where feature widths and heights are measured with nanometer precision. An important factor here is to take into account the geometrical interaction between the tip shape (conical, pyramidal) and the surface features (high-aspect ratio features). In general, the obtained topographic contours are a convolution between the two shapes. It is therefore important to know exactly the tip contour in order to interpret the obtained image. Fig. 2.10 shows an SFM image taken with one of our silicon cantilevers of a fraction of a microfabricated Fresnel lens, a miniaturized diffractive optics element (DOE). The sample material is glass that has been etched with an ion milling process to etch the steps of different heights. The maximum profile is about 1 μm with step widths of about 10 μm. (Image courtesy of M. Binggeli, CSEM S.A., Neuchâtel).

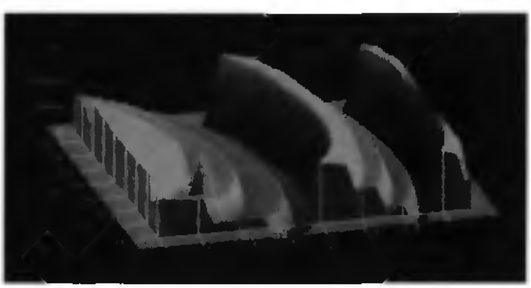

Fig. 2.10 Contact mode SFM image of an etched Fresnel lens for DOE applications. Structure height ≅ 1 μm, step width ≅ 10 μm. Image taken by M. Binggeli, CSEM S.A. Neuchâtel.

Non-contact mode imaging

In the non-contacting mode, the cantilever is vibrated near its resonance frequency. When approaching surface features, the force gradient acting onto the cantilever changes its vibration characteristics, resulting in a change in amplitude and phase. Fig. 2.11 shows the SFM image of a gold-covered mica sample, which has been recorded by measuring the changes of the amplitude with an optical beam deflection system. (Image courtesy of M. Jobin, Université de Genève).

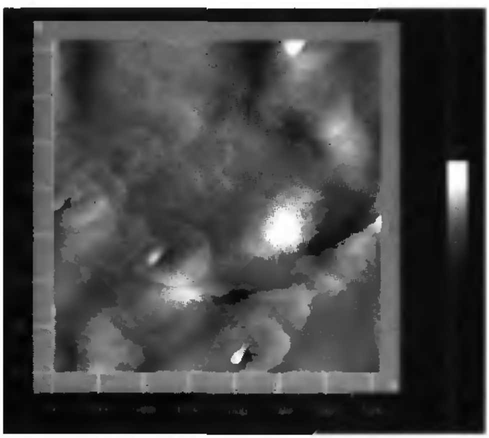

Fig 2.11: Non-contact mode image of gold on mica. The force gradient induced amplitude change of the lever vibration were measured by optical beam deflection. Image courtesy of M. Jobin, University of Geneva.

STM with a diamond coated silicon tip

One of our silicon cantilever-tip was post-processed and CVD coated with a thin doped diamond layer. Ph. Niedermann from the CSEM S.A. used such a tip for STM experiments[19]. Fig. 2.12 (left) shows a SEM micrograph of the prepared tip. Fig. 2.12 (right) shows an image of a Au <111> film taken in STM mode with the diamond tip. The vertical scale is 8 nm and the scan window is 200 x 200 nm^2. Using a cantilever for STM experiments can be advantageous compared to normal metal tips, since the risk of a ramming the into the surface is reduced because of the flexibility of the cantilever. In addition, an independent force feedback can be used simultaneously.

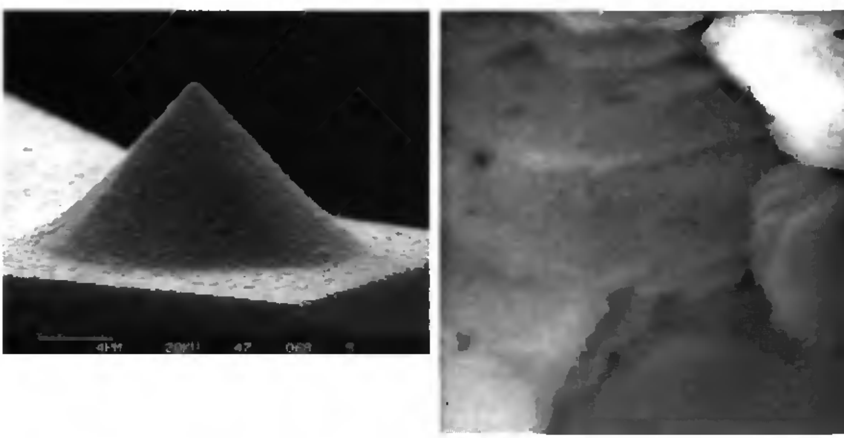

Fig 2.12: (left) SEM micrograph of the diamond coated silicon tip; (right) STM image using the diamond coated silicon cantilever-tip. The sample is a <111> Au film., the vertical scale is 8 nm, the scan range is 200 nm x 200 nm. Image courtesy of Ph. Niedermann, CSEM S.A. Neuchâtel.

Surface modification with the scanning probes

If the interaction between the tip and the sample is strong enough, the tip will modify the surface, a technique often referred to as, nano-indentation. Potential applications are high-density lithography and data-storage. The kind of interaction can vary from electrical, magnetic or simply mechanical.

A nice application of a mechanical surface modification is for instance the patterning of a polymer layers for the fabrication of liquid crystal devices. Scratching the polymer creates an anisotropic surface morphology that aligns liquid crystal molecules. Normally this procedure is done by a rubbing process on large scale. Using the tip of a SFM allows the fabrication of arbitrarily shaped refractive index patterns in the liquid crystal on the μm scale. The SFM is operated at high loads of up to 10^{-5} N, thus stiff cantilevers are required. By using an array of cantilever-tips as shown in Fig. 2.13, parallel wave guides can be fabricate in a single process with high accuracy.

Martin Rüetschi from the University of Basel has used an area of our most stiff cantilevers to pattern parallel liquid crystal wave guides in polymer[20]. Fig. 2.14 shows the polarizing image, taken with an optical microscope of a liquid crystal cell with a series of gratings. The horizontal rows have been fabricated simultaneously with an array of 10 cantilevers. The periodicity of the gratings from left to right are 10, 8, 6, 4 μm. The height of the structure is 21 μm. Regions which were modified by the scratching process appear bright because of the twisted structure of the liquid crystals.

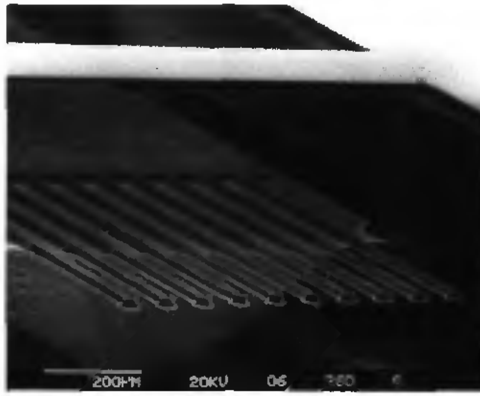

Fig 2.13 SEM micrograph of a microfabricated array of silicon cantilevers with tips as used for the parallel scratch indentation experiment.

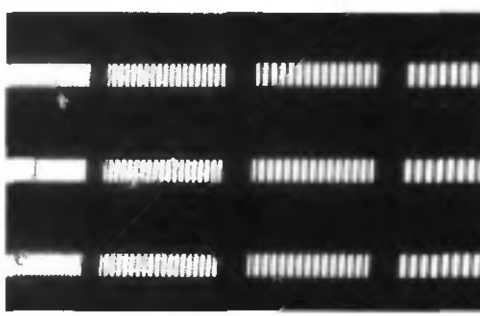

Fig 2.14: Polarizing microscope image of an liquid crystal cell. The series of gratings have been patterned simultaneously with a 10 cantilever array. The grating periodicity from left to right is 10, 8, 6, 4 µm. The structure is 21 µm high. The bright light shows where the polymer has been scratched which results in a twisting of the liquid crystals. Image courtesy of M. Rüetschi, University of Basel.

2.5 Conclusions

In this chapter we have shown that SFM cantilevers and tips can be micromachined by a mass-fabrication silicon dissolving process. Photolithographic techniques allow for the fabrication of different cantilever dimension in a single batch process. Selective etching (dry and wet) sculpture the tiny silicon cantilevers with integrated tips out of the silicon bulk. Low temperature oxidation has been used to achieve ultra-sharp tips with radii of less than 2 nm. The feasibility of multiple probes arranged in an array has been demonstrated. The etching of a tip array exhibits some irregularities in terms of tip shape due to a non homogenous etch rates at the border of the array. Dummy structures are a possible remedy to obtain regular working tip arrays. The fabricated device have been used successfully in standard SFM equipment in contact SFM, non-contact SFM, STM, and surface modification mode. If a multiple tip array for parallel surface imaging is aimed at, then we need to integrate an active feedback for each cantilever probe. The following chapters will discuss this topic.

---

[1] T.R. Albrecht and C.F. Quate; J. Vac. Sci. Technol. A 6(2), Mar/Apr 1988, 271-274

[2] e.g. B. Hübner, H.W.P. Koops, H. Pagnia, N. Sotnik, J. Urban, M. Weber; proceedings STM 91

[3] O. Wolter, Th. Bayer and J. Greschner; J. Vac. Sci. Technol. B9, 1991, pp. 1353

[4] T. Ishitani, T. Ohnishi and Y. Kawanami; Jap. J. Appl. Phys. 29, 1990, pp. 2283-2287

[5] T.R. Albrecht, S. Akamine, T.E. Carver, C.F. Quate; J. Vac. Sci. Technol. A8, 1990, p. 3386

[6] catalogue of OLYMPUS OPTICAL CO., Japan

[7] S. Akamine and C.F. Quate; J. Vac. Sci. Technol. B 10(5), Sep/Oct 1992, 2307-2310

[8] S. Akamine, R.C. Barrett and C.F. Quate; Appl. Phys. Lett. 57 (3), 16 July 1990, p. 316

[9] O. Wolter, Th. Bayer and J. Greschner; J. Vac. Sci. Technol. B9, 1991, pp. 1353

[10] R.A. Buser, J. Brugger, N.F. de Rooij; Transducers '91, San Francisco, Techn. Digest p. 249-252

11 P.C. Allen; Inst. Phys. Conf. Ser. No 99: Section 2; 2nd Int. Conf. on Vac. Microelectron., Bath 1989, p. 17

12 Y. Martin, H.K. Wickramasinghe, Appl. Phys. Lett. 64 (19), May 9, 1994

13 R.B. Marcus et al.; Appl. Phys. Lett. 56 (3), 15 January 1990, p. 236

14 C. Linder, T.Tschan, N.F. de Rooij; Proceedings Transducers '91, p.524

15 S.C. Minne, Ph. Flueckiger, H.T. Soh, C.F. Quate; to be published in J. Vacuum Science and Technology B (May/June 1995)

16 V.K. Singh, E.S.G. Shaqfeh, J.P. McVittie; J. Vac. Sci. Technol. B10(3), May/Jun 1992, p.1091

17 S. Hoen, O. Züger, C.S. Yannoni, H.J. Mamin, K.Wago, D. Rugar; Solid-State Sensor and Actuator Workshop, Hilton Head, SC, June 13-16, 1994, p. 209

18 J.E. Griffith, D.A. Grigg; Applied Physics Review (1993)

19 Ph. Niedermann, W. Haenni, N. Blanc, R. Christoph, J. Burger; to be published in J. Vac. Sci. Technol.

20 M. Rüetschi, H.-J. Güntherodt, P. Grütter, J. Fünfschilling, to be published in 'Photons and Local Probes', Kluwer Academic Publisher, NATO ASI series E: Applied Sciences.

Chapter 3

Capacitive microlever

This chapter discusses the microfabricated capacitive microlever for the SFM. The device represents an attractive way for the integration of a cantilever deflection sensor. In addition it can serve as a micro-actuator for inducing cantilever motion for adjusting the tip to sample distance, thus representing an interesting asset for multiple probe systems where individual tip control is required.

Among all types of electrical devices the capacitor is probably the oldest one. The original definition of capacitance has been given by Maxwell in 1873. It states that the potential difference V across a capacitor is proportional to the charge Q, or $V = Q/C$. The proportionality factor $1/C$ is the inverse of the object capacitance. The capacitance of a parallel plate capacitor is given by $C = \varepsilon_0 A/d$, where ε_0 is the permittivity of vacuum, A is the area and d is the gap. Changing either A or d (or both) results in a variation of C. This concept is used in numerous displacement sensors, where one electrode is kept fixed and the other is allowed to move. The resulting change of d or A can be monitored very precisely[1,2].

Microfabricated capacitive accelerometers have already been introduced in the early 1980s by Rudolf and coworkers at the CSEM Neuchâtel[3]. They are now widely utilized in commercial products, since capacitive detection is known for its high sensitivity and good immunity to thermal noise, when compared to, e.g., piezoresistive sensors.

For the field of scanning force microscopy the idea of capacitive sensing for the cantilever motion has first been suggested in 1987 by Binnig and coworkers[4] at IBM Rüschlikon. Later in 1990, Göddenhenrich and coworkers[5] at the Kernforschungsanlage Jülich demonstrated experimentally the feasibility of capacitive deflection detection. They used 5 mm long aluminum wires of 25 μm diameter as levers and achieved a sensitivity of 0.1 fF/Å by using a capacitance transformer bridge.

Also in 1990, Neubauer and coworkers[6] at IBM Almaden presented a bi-directional capacitance force sensor for the simultaneous recording of normal and lateral forces to determine the tribological properties of surfaces. Their structure consisted of an assembly of micromachined silicon and glass components. In their work they achieved a sensitivity of 0.39 fF/Å by using a radio frequency detection circuit.

Despite its early presence in the family of the cantilever deflection sensors the capacitive approach did not get the same credits as the today most popular method of using optical beams. This is probably due to following reasons: first, the assembling of the capacitor electrode plates with micrometer precision is a rather critical and unreliable technique compared to the relative easy adjustment of an optical beam, and second, achieving high-resolution with a capacitive set-up is more critical due to stray capacitance effects, compared to optical techniques.

The capacitive sensing method may probably revive if we are successful by building more accurate, reliable and reproducible devices. At the IMT we developed a new type of capacitive microlever with self-aligned electrodes that are fabricated by a silicon microfabrication process. It is possible to cost effectively produce large numbers of such devices in a single wafer batch process. In addition parallel probes with integrated sensors and actuators become feasible with this technique. For parallel operation of several probes it is mandatory to have addressable tips in an array with individual sensing *and* actuation capabilities.

The following paragraphs first describe the design of the capacitive microlevers and then give a theoretical analysis of their sensing and actuation capabilities. The microfabrication sequence and experimental of the device characteristics are then presented.

3.1 Design of the capacitive microlever

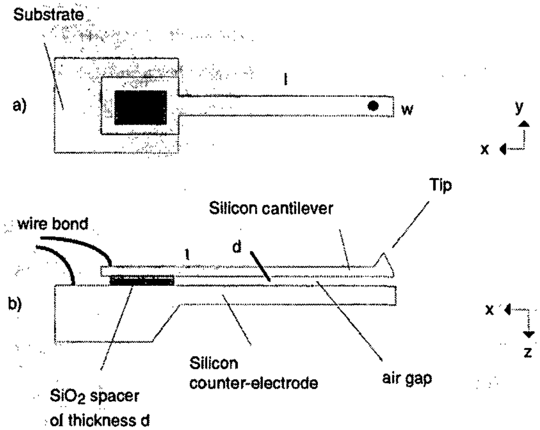

Fig. 3.1: Illustration of the capacitive microlever; a) top view, b) side view,

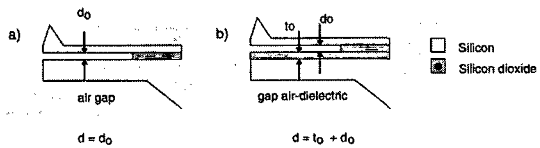

Fig. 3.2: a) pure air gap of width $d = d_O$, (b) gap of air and silicon dioxide with a total width of $d = t_O + d_O$

The microfabricated capacitive microlever consists of a cantilever, carrying a sharp tip, and an adjacent counter-electrode, attached to the substrate holder. They form a parallel plate capacitor. A schematic representation of the device is shown in Fig. 3.1. The cantilever beam, the tip, the counter-electrode and the support holder are made of single-crystal silicon. The dielectric anchor pad between the electrodes is made of thermal silicon dioxide. The simplest possible shape of such a device are two rectangular beams. The counter-electrode is considerably thicker than the force sensing cantilever so that it is not influenced by forces.

The mechanics for such a cantilever can be derived from chapter 1. The spring constant and the resonance frequency are given by $k_z = 3\,E\,I / l^3$ and $f = 1/2\pi \sqrt{k_z / m_{eff}}$, respectively, where $I = w\,t^3/12$ is the cross sectional moment of inertia, $E = 1.7 \times 10^{11}$ N/m^2 is the Young's modulus for silicon, and m_{eff} is the effective cantilever mass ($m_{eff} \approx 0.24$ m).

The capacitance C_S of the parallel plate capacitor formed by the lever and the counter-electrode is given by

$$C_S = \frac{\varepsilon\, w\, l}{d} \tag{3.1}$$

where $\varepsilon = \varepsilon_r\, \varepsilon_o$ with $\varepsilon_o = 8.85 \times 10^{-12}$ As/Vm. ε_r depends on the material between the electrodes. With the silicon technology that we have used we can fabricate the capacitive gap by different ways. Two possible situations are shown in Fig. 3.2., in (a) a pure air gap (ε_r = 1) of width d_o between the two silicon electrodes, and in (b) a mixed gap of air and silicon dioxide ($\varepsilon_r = 3.9$) with a total thickness $d_o + t_o$.

In the case of (b) the total capacitance of the device becomes

$$C_S = \frac{\varepsilon_o \varepsilon_r w\, l}{\varepsilon_r\, d_o + t_o} \tag{3.2}$$

and if $d_o = t_o = d/2$

$$C_S = \frac{2\, \varepsilon_o\, \varepsilon_r\, w\, l}{d\, (\varepsilon_r + 1)} \tag{3.3}$$

When comparing the air gap and the mixed gap air-SiO_2 we find that, for an identical total gap d between the silicon electrodes the mixed gap air-dioxide has the advantage of increasing the capacitance by nearly 60%. On the other hand it reduces by 50 % the vertical excursion range of the tip. This structure, however, incorporates an additional advantage: when the tip excursion exceeds the allowed gap of d_o and the cantilever touches the counter-electrode, we have a short circuit in (a) but not in (b).

In an experimental set-up the total capacitance of the microlever is composed of three contributions: the sensor capacitance C_S, the capacitance C_p of the dielectric anchoring pad and the capacitance C_b of the bonding interconnections that lead to the interface electronics. Since they are parallel to each other we obtain for the total measurement capacitance the sum of the capacitance $C_{tot} = C_S + C_p + C_b$.

We designed the 'capalevers' to have typical dimensions of: 140 - 800 µm in length and 40 µm in width, which yields an area A of 5600 - 32'000 µm^2. With these lateral dimensions and a gap of 3 µm, we obtain a sensing capacitance C_S between 16.5 fF and 94 fF. C_p and C_b

are in the order of 1 - 3 pF. They are thus about one order of magnitude larger than C_S. We use following values to calculate C_P: capacitance area $A_P = 100 \times 100\ \mu m^2$, gap $d_{ox} = 3\ \mu m$.

For high sensitivity it is required to have C_S as large as possible. If we can decrease the gap d to about 1 µm, then we obtain values for C_S between 49.6 fF and 283 fF. A further decrease of d below 1 µm would further increase the sensor signal. However the fabrication reaches the technological limits. And in addition there are also functional reasons not to use a too small gap because of the already mentioned excursion limit of the tip displacement, and also by the broadening of the resonance due to air squeezing effects (for a vibrating cantilever operated under atmospheric pressure).

For applications in scanning force microscopes we therefore have to find a trade off between the mechanical and the electrical requirements. In our work here we were successful in fabricating devices with air gaps d of typically 3 µm. In the next paragraph we show that with these dimensions we obtain an interesting device for lever actuation by electrostatic forces. And we will also learn that the integrated deflection sensing method shows relatively poor performance in the static, but promising results in the dynamic mode.

3.2 Analysis of the actuator function

S t a t i c   d e f l e c t i o n

When we apply an electrostatic field between the electrodes of a capacitor we create electrostatic forces. In the case of a parallel plate capacitor with an area A, a gap d and an applied voltage V, the electrostatic force F_{el} is given by

$$F_{el} = \frac{1}{2} \varepsilon_0 \frac{A}{d^2} V^2 \qquad (3.4)$$

In the present case (a cantilever clamped at one end and free at the other end), a mathematical complication comes from the deflection of the cantilever and the non-uniform electrostatic forces present along its length. For small displacements of the tip ($z_0 \ll d$) however, the cantilever senses approximately a constant electrostatic pressure[7]

$$P_{el} = \frac{1}{2} \varepsilon_0 \frac{V^2}{d^2} \qquad (3.5)$$

This leads to a displacement of the tip given by[8]

$$z_0 = \frac{1}{16} \varepsilon_0 \frac{V^2}{d^2} \frac{w\, l^4}{E\, I} \qquad (3.6)$$

On the other hand, for a concentrated electrostatic force F_c

$$F_c = \frac{1}{2} \varepsilon_o \frac{A_{eff}}{d^2} V^2 \qquad (3.7)$$

acting at the end of the cantilever, the displacement is then given by

$$z_o = \frac{1}{6} \varepsilon_o \frac{A_{eff} V^2}{d^2} \frac{l^3}{E I} \qquad (3.8)$$

The comparison of equations (3.6) and (3.8) shows that the same tip displacement is obtained provided one defines an effective area $A_{eff} = (3/8)$ wl. Within this approximation it is straightforward to predict the cantilever deflection as a function of the applied bias voltage.

An elegant method to describe the overall behavior of the device to applied voltages is to compute the total potential energy U_{tot} of the system, which is determined by two conservative forces[7,9]: the electrostatic driving force F_{el} and the restoring spring force $F_{spr}(z) = kz$. The total potential energy of the beam actuator can be expressed as the sum of the strain energy of the deflected cantilever and the electrostatic energy due to the driving voltage V:

$$U_{tot}(z) = U_{spr}(z) + U_{el}(z)$$

$$= \frac{1}{2} k z_o^2 - \frac{1}{2} \varepsilon_o \frac{A_{eff}}{d - z_o} V^2. \qquad (3.9)$$

This equation is significant and deserves emphasis. It yields information on both the cantilever displacement and the stability conditions. The cantilever equilibrium positions, for instance, are found by solving

$$\frac{dU_{tot}}{dz} = 0 \qquad (3.10)$$

which yields

$$k z_o = \frac{1}{2} \varepsilon_o \frac{A_{eff} V^2}{(d - z_o)^2} \qquad (3.11)$$

i.e. the spring restoring force equals the electrostatic force. These two opposite forces generate a stable position of static equilibrium at the minimum (U_{min}) and an unstable equilibrium at the maximum (U_{max}) of the potential energy curve, respectively (Fig. 3.3). When the applied voltage exceeds a certain threshold voltage V_t no stable equilibrium position exists and the second derivative d^2U_{tot}/dz^2 becomes *always* negative. This case reflects the situation when the cantilever's own mechanical spring constant is too small to be able to withstand the attractive electrostatic force and the lever 'snaps' into the counter-electrode. The snapping distance z_t and voltage V_t can easily be computed by satisfying $dU_{tot}/dz\ (z=z_t) = 0$ and $d^2U_{tot}/dz^2\ (z=z_t) = 0$. The snapping distance is given by

$$z_t = \frac{d}{3} \tag{3.12}$$

and the threshold voltage is given by

$$V_t = \sqrt{\frac{8\, d^3\, k}{27\, \varepsilon_0\, A_{eff}}} \tag{3.13}$$

Hence, the actuation range of the cantilever is limited to *one third* of the inter-electrode gap d. For a typical cantilever (l = 800 µm, w = 40 µm, t = 5 µm) and a gap of 3 µm gap we obtain a snapping voltage of $V_t \cong 5.5$ V and an operation range of $z_t = 1$ µm. The threshold voltages for various device dimensions are summarized in Table 3.1 at the end of paragraph 3.3.

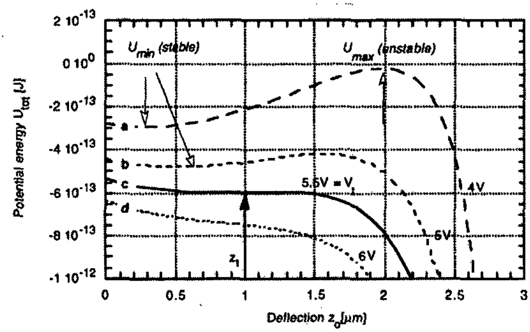

Fig. 3.3: The calculated total potential energy U_{tot} as a function of z_0 for the capacitive microlever with typical dimensions (l = 800 µm, w = 40 µm, t = 5 µm, d = 3 µm) showing the equilibrium positions. Threshold voltage $V_t \cong$ 5.5 V and snapping distance z_t = 1 µm [7,9]

Effective spring constant

The cantilever compliance k is changed by the electrostatic forces. Using the same model as before we can express the resulting effective compliance k' as a function of the applied bias voltage V by

$$k'(V) = \frac{d^2 U_{tot}}{dz_o^2}$$

$$= k - \frac{\varepsilon_o A_{eff}}{(d - z_o)^3} V^2 \qquad (3.14)$$

For $V = V_t$ we obtain $k'(V_t) = 0$. At the threshold point the stiffness of the cantilever is zero. With the electrostatic field we can adjust the force constant of the cantilever from the mechanical compliance k down to k' = 0 in a controlled way.

The described control over the cantilever stiffness opens new fields in scanning force microscopy, where stiff levers are needed for imaging large force gradients, but where soft levers in general show a better force sensitivity. A cantilever with a tunable compliance would allow to meet these contradictory requirements.

The lowering of the compliance k is also reflected in a lowering of the resonance frequency f_o' of the cantilever. According to equation (1.2) we obtain

$$\frac{f_o'(V)}{f_o} = \sqrt{\frac{k'}{k}}$$

$$\cong 1 - \frac{4}{27}\left(\frac{V}{V_t}\right)^2. \qquad (3.15)$$

As a numerical example: for a dc voltage of 1 Volt, a typical cantilever (with f_o = 11 kHz, k = 0.4 N/m and V_t = 5.6 V) changes the frequency by 52 Hz and the spring constant by about 0.004 N/m.

Dynamic deflection

We assume now a sinusoidal field $V_{ac} \cos \omega t$ superimposed to the V_{dc} applied between the counter-electrode and the cantilever. The first order Taylor expansion of the electrostatic force F_{el} yields

$$F_{el} \cong \frac{1}{2} \varepsilon_o \frac{A_{eff}}{d^2} (V_{dc}^2 + 2V_{dc}V_{ac} \cos \omega t) \qquad (3.16)$$

where we assume that $V_{ac} << V_{dc}$ so that higher-order terms do not contribute significantly. This term yields the forced vibrations of a cantilever due to the driving electrostatic voltage. The net oscillating force exerted on the cantilever is then given by

$$F_{el} \cong \varepsilon_o \frac{A_{eff}}{d^2} V_{dc}V_{ac} \cos \omega t \qquad (3.17)$$

The equation of motion of the cantilever due to F_{el} can be expressed by

$$m_{eff}\frac{d^2z}{dt^2} = -k' z - c\frac{dz}{dt} + \varepsilon_0 \frac{A_{eff}}{d^2} V_{dc} V_{ac} \cos \omega t \qquad (3.18)$$

where m_{eff} is the effective mass of the lever, k' denotes the effective lever compliance as a result of the applied dc voltage according to equation (3.15), and c is the coefficient of the viscous damping. In the steady state the displacement z from the static equilibrium position is given by the standard resonance equation[10]

$$z = \varepsilon_0 \frac{A_{eff}}{k\,d^2} V_{dc} V_{ac}\, \beta \cos(\omega t - \theta) \qquad (3.19)$$

in which the magnification factor is

$$\beta = [(1-\omega^2/\omega_0^2)^2 + (\omega/Q\omega_0)^2]^{-1/2} \qquad (3.20)$$

and the phase angle is

$$\theta = \tan^{-1}\left(\frac{\omega/Q\omega_0}{(1-\omega^2/\omega_0)}\right) \qquad (3.21)$$

with the quality factor $Q = m_{eff}\omega_0/c$.

3.3 Analysis of the sensor function

Quasi-static (or contact) mode

We determine now the sensing capabilities of the capacitive microlever for scanning force microscopy. In the present case we assume the lever in a quasi-static motion which is *not* vibrated. When raster scanning the tip across a sample local surface interaction induce minute deflection z of the cantilever beam. The elastic curve of the lever with spring constant k due to such a concentrated load F at the end can be expressed by

$$z(x) = \frac{z_0}{2\,l^3}(x^3 - 3\,l^2\,x + 2\,l^3) \qquad (3.22)$$

where $z_0 = F/k$ is the deflection at the free end (x=0). This cantilever motion changes the air-gap capacitance C_s according to

$$C_s(z_0) = \int_0^l \frac{\varepsilon_0 w}{d - z(x)}\, dx \qquad (3.23)$$

Ultimately, the sensitivity is governed by the capacitance derivative $\delta C_S/\delta z_O$, and for small deflections ($z_O << d$) around the relaxed position it can be expressed in an analytical form as

$$\frac{\delta C_S}{\delta z_O}(z_O=0) = \varepsilon_O \frac{3wl}{8d^2} \tag{3.24}$$

This corresponds to the sensitivity for a simple parallel-plate capacitor where the electrodes are approached on their full length by defining an effective area of $A_{eff} = 3/8$ w l.

This is easily understood, the cantilever being a one-side clamped beam which is only free to bend near the tip, and therefore only a fraction of the area A contributes to the changes in capacitance. It corresponds to the result obtained in the previous paragraph for the deflection actuation. By using numerical calculations the sensitivity $\delta C_S/\delta z_O$ can be computed around any tip displacement z_O.

For a microfabricated capacitive microlever (l = 800 μm, w = 40 μm and d = 3 μm) we obtain a capacitance derivative of $\delta C_S/\delta z_O \cong 10$ aF/nm (aF = attofarad = 10^{-18} F). Fig. 3.4 shows the calculated sensitivity for this type of device as a function of z_O for different gap values (d = 1 - 3 μm) for both, positive and negative deflections.

In a typical capacitance measurement set-up an oscillating voltage is applied across the capacitor and the reactive current is measured. In principle, a very good signal-to-noise ratio (S/N) and precise measurements is possible since the capacitor has no Johnson noise (associated with resistors) and no shot noise (associated with semiconductor junctions). However, the evaluated sensitivity of 10 aF/nm is about 2 orders of magnitude lower than reported by Göddenhenrich and Neubauer, who both used significantly larger structures. A dedicated and very sensitive electronic circuitry is indeed required in order to obtain atomic resolution.

We therefore believe that the capacitive microlever with the given small dimensions is not so suitable for SFM in the static or contact mode.

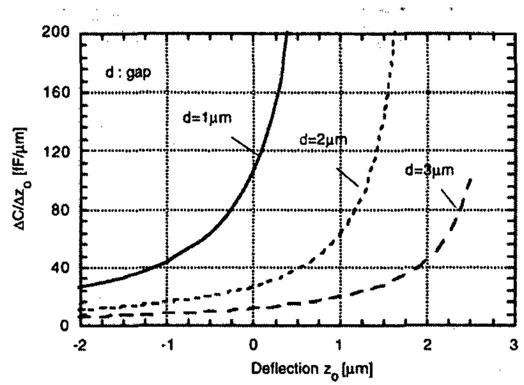

Fig. 3.4: Calculated sensitivity $\Delta C/\Delta z_0$ of the capacitive microlever as a function of z_0 for different gap values (d = 1 - 3 µm); l = 800 µm, w = 40 µm, positive and negative deflection are shown.

Dynamic (or non-contact) mode

Another method for surface force measurements is to put the cantilever into vibrations and to detect changes of the resonance by using phase sensitive techniques. This method is particularly interesting for non-contact mode imaging of force gradients. A typical application is magnetic force microscopy. In common systems the cantilever vibration is induced by a PZT actuator onto which the probe is mounted. Force gradients that change the effective spring constant k of the system to $k' = k + \delta F'$ are detected through shifts in the resonance frequency or amplitude of the mechanical vibration of the cantilever, and are commonly measured by using an interferometer or beam deflection set-up.

Albrecht and coworkers[11] have shown that by using frequency modulation (FM) techniques, the minimum detectable force gradient is given by

$$\delta F'_{min} = \sqrt{\frac{4\,k\,k_B\,T\,B}{\omega_0\,Q < z_{osc}^2 >}} \qquad (3.25)$$

where k is the cantilever spring constant, k_B is the Boltzman constant, T is the temperature, B is the measurement bandwidth, ω_0 is the frequency, Q is the quality factor, and $<z_{osc}^2>$ is the mean-square amplitude of the self-oscillating cantilever. The minimum detectable force gradient for the cantilevers of the capacitive devices are summarized in Table 3.1. They amount to typically 3×10^{-4} N/m in a bandwidth B = 1 kHz, at room temperature and when assuming Q = 2000 with a rms vibration amplitude of 1 nm.

With $k' = k + \delta F'$ and equation (3.15) we can calculate the new frequency f' according to

$$f' = \sqrt{1 + \sqrt{\frac{4\, k_B\, T\, B}{2\pi\, f\, Q\, \langle z_o^2 \rangle}}\, \frac{1}{k}}\;\; f \qquad (3.26)$$

The values for the corresponding frequency change $\Delta f = f - f'$ are listed in Table 3.1. They amount typically to 1 to 4 Hz, with the same experimental conditions as above. According to equation (3.7) we can compute the minimum equivalent voltage change ΔV_{min} that corresponds to $\delta F'_{min}$ which lies in the order of several mV.

Table 3.1 *Dimensions and calculated characteristics of 4 typical capacitive microlevers*

capacitive lever	length l [µm]	width w [µm]	k [N/m]	f_0 [kHz]	C_s [fF]	$\Delta C/\Delta z$ [aF/Å]	V_t [V]	$\delta F'_{min}$ [N/m]*	Δf [Hz]*	ΔV min [mV]*
1 (t=3µm, d=1µm)	140	40	16.7	213.9	49.6	1.9	16.3	3.21 E-04	2.05	6.0
2	325	40	1.3	39.7	115.1	4.3	3.0	2.11 E-04	3.12	3.1
3	425	40	0.6	23.2	150.5	5.6	1.8	1.84 E-04	3.57	2.6
4	800	40	0.1	6.6	283.2	10.6	0.5	1.34 E-04	4.90	1.6
1 (t=5µm, d=1µm)	140	40	77.4	356.4	49.6	1.9	35.1	5.35 E-04	1.22	7.6
2	325	40	6.2	66.1	115.1	4.3	6.5	3.51 E-04	1.87	4.0
3	425	40	2.8	38.7	150.5	5.6	3.8	3.07 E-04	2.14	3.3
4	800	40	0.4	10.9	283.2	10.6	1 .1	2.24 E-04	2.94	2.1
1 (t=3µm, d=3µm)	140	40	16.7	213.9	16.5	0.2	84.9	3.21 E-04	2.05	17.6
2	325	40	1.3	39.7	38.4	0.5	15.7	2.11 E-04	3.12	9.4
3	425	40	0.6	23.2	50.2	0.6	9.2	1.84 E-04	3.57	7.7
4	800	40	0.1	6.6	94.4	1.2	2.6	1.34 E-04	4.90	2.1
1 (t=5µm, d=3µm)	140	40	77.4	356.4	16.5	0.2	182.6	5.35 E-04	1.22	22.8
2	325	40	6.2	66.1	38.4	0.5	33.9	3.51 E-04	1.87	12.1
3	425	40	2.8	38.7	50.2	0.6	19.8	3.07 E-04	2.14	9.9
4	800	40	0.4	10.9	94.4	1.2	5.6	2.24 E-04	2.94	6.2

* calculated values according to the equations (3.25), (3.27) and (3.28) with B=1kHz, Q=2000, $\langle z_{osc}^2 \rangle$ = 1 nm, T = 300 K

3.4 Microfabrication - The aligned wafer bonding technique

This paragraph describes the fabrication steps for the micromachined capacitive microlever. The fabrication is based on the process for the simple silicon cantilever with tips but is extended by an essential additional step: the *aligned wafer bonding*. This step is a relatively new microfabrication step and we will consider it in more detail in this paragraph. Recently, more and more microfabricated sensor and actuator devices rely on this technique which is useful in cases where two or more bulk structures have to be placed extremely close to each other with a precise gap separation. Micromachined pressure sensors and accelerometers using capacitive measurement principles are often fabricated using this technique[12].

Many capacitive micro-devices are fabricated by the so-called surface micromachining process with sacrificial layer etching technology. The structure materials are typically chemical vapor deposited thin films (poly-silicon) with an underlying sacrificial layer (e.g. silicon dioxide). Poly-silicon, as deposited, for micromechanical applications has a thickness of typically 1 - 3 μm and is therefore not well suited for making cantilever with tips (requiring an overall thickness of 5 - 10 μm). Furthermore, the formation of tip like structures by the mask under etching as described in chapter 2 for single-crystal silicon is not observed for poly-silicon.

We therefore developed a new process for the capacitive device and use a bonding step to bring the counter-electrode and the cantilever closely spaced together within the desired gap width of about 1 - 3 μm.

In general at least two ways exist for making a precise air-gap. The first method is to bond the structures together by using an oxide interface and to remove subsequently this sacrificial layer. The gap hereby is determined precisely by the thickness of the interface layer. The second method is to pattern the bond-oxide to specific pads prior to the bonding. In such a case the sacrificial layer etching becomes obsolete which is a considerable process improvement in terms of device yield and reproducibility.

In our first version we have used the sacrificial layer method and obtained a yield of only ≅ 20% working devices. We believe that the major problem lies in the inhomogenous bond strength over a large surface area. The bonded pads can withstand strengths due to mechanical forces very well. This could be observed by a razor blade test on wafer level. However, when wet chemical etching such as buffered HF is used to laterally etch the oxide, then capillary forces increase the lateral etch rate to an uncontrollable amount such that large areas are under etched and released before the oxide is completely removed between the sensor electrodes. Fig. 3.5 illustrates this effect.

We therefore extended and improved the process by an additional mask step which defines the actual bond areas, and with this precisely the dielectric pad capacitors c_p which are in parallel to the capacitive microlever. With this technique the critical step of sacrificial layer etching becomes obsolete and a yield of about 70 % could be obtained.

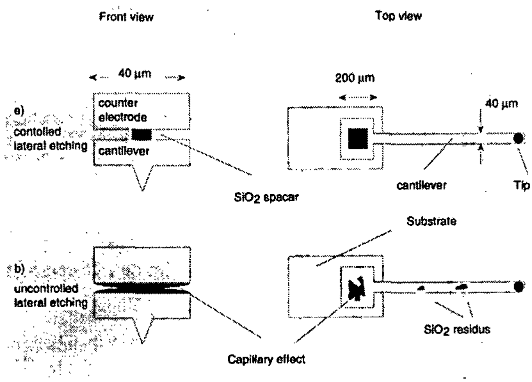

Fig. 3.5: Illustration of the sacrificial etching of the capacitor air-gap when using thermal dioxide as bond interface; (a) good bond quality, the lateral etch rate can be controlled, (b) poor bond quality, uncontrolled lateral etch rate due to capillary forces

The process steps

The fully batch compatible process is illustrated in Fig. 3.6. We use two 3 inch (100) double side polished, 280 µm thick silicon wafers which are n-type doped to have a bulk resistivity of 0.03 Ω-cm. The upper wafer is used to build the cantilever, the lower wafer is used to build the counter-electrode and the support handle, respectively. An oxide layer of 1.5 µm is grown thermally which serves as etch mask for the subsequent dry and wet etch steps.

The upper wafer is photographically patterned and the oxide is etched in BHF to the cantilever shapes. RIE using C_2ClF_5/SF_6 gases is used to etch trenches of 5 - 10 µm into the silicon surface. The depth of this etch step basically defines the thickness of the cantilevers although the exact thickness will also be determined later during the final dry and wet etching of the tip. Generally the final thickness of the cantilever can be tailored to about 3 - 7 µm depending on the various etch processes.

The lower wafer is patterned in a similar way. Here a double side process is used to pattern the oxide. On the front side bond pads are structured exactly there where the wafer will be fusion bonded together. They form the anchor points between the two wafers and thus a frame for stability and, more important, they define the capacitor plates that are in parallel to the sensing capacitor. It is therefore important to minimize those pads but still keep them big enough to ensure a stable mechanical link (!) between the cantilever and the counter electrode on the handle. On the back side of the lower wafer windows with compensation structures are opened in the oxide for the anisotropic wafer back etching. Thick photoresist (in our case we used 8 µm thick AZ 4562) is then spun over the oxide pads on the front side and patterned to the shape of the counter electrodes. RIE is used to etch deep trenches of 10 - 15 µm into the silicon. We want the counter electrodes to be much thicker than the cantilevers, therefore the deeper etching.

After the resist stripping and prior to the contacting and fusion bonding the wafer surfaces are carefully cleaned and hydrophilized. We use a standard surface cleaning and bond preparation procedure[13] with HNO_3, H_2SO_4:H_2O_2 and DI water rinsing cycles. After drying in N_2 atmosphere the wafers are loaded on a commercial mask and bond aligner[14].

The two bond partners are optically aligned and immediately put into contact, face to face. The pre-structured cantilevers and counter-electrodes are here 'sandwiched' between the wafers (Fig. 3.6b). An alignment accuracy of less than 2 µm can be achieved. This is better than what can be obtained with infrared assisted bond aligners with a resolution limit of about 5 µm[15]. In our typical devices the active bond pads form areas of some 100 µm x 100 µm. This is a rather small area for usual bonding techniques. A misalignment would also cause the counter-electrode and cantilever to be displaced laterally to each other which would affect the capacitance area A and decrease the sensitivity. By enlarging the shape of the counter-electrode with respect to the cantilever, this risk can be reduced.

After the contacting of the bond partners hydro-bond forces resulting from the surface treatment are sufficient to preliminary 'pre-bond' and glue the wafers together. The actual fusion bonding is subsequently performed in an annealing furnace in O_2 or N_2 atmosphere at 1100 °C during about 4 h.

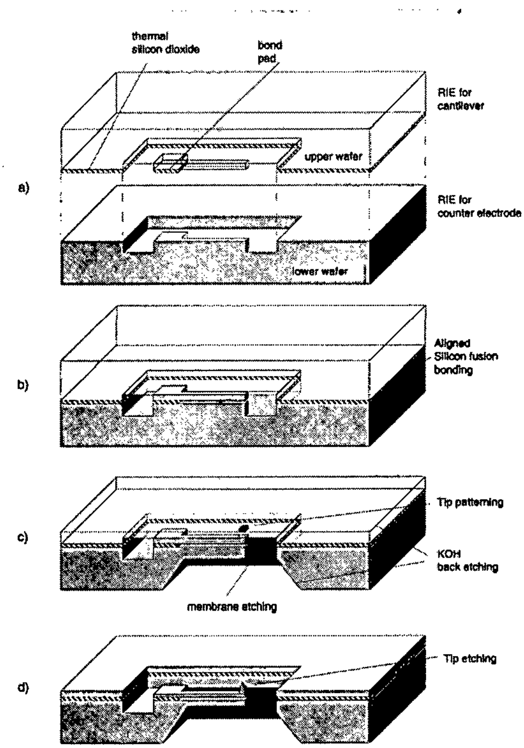

Fig. 3.6: Microfabrication steps of the capacitive microlever

For the back-etching we use our standard KOH process as described in Ch. 2. Again the back etching is time controlled to stop at a membrane of roughly 20 μm. The KOH also etches on the upper wafer and removes most part of the bulk silicon. An approximately 5-10 μm thick membrane is now covering the cantilever hidden under the fine membrane which is later used to build the tips.

The tip etching is performed with the deposition of a masking layer and subsequent RIE step. In the first experiments we successfully used a thermally grown oxide, which however is a critical high temperature process at this stage for the fragile devices. We also tried to use a layer of thick photoresist which has shown to be sufficient for the etching of silicon tips.

Simultaneously during the etching of the tip we etch down and finally remove the topside silicon membrane which is covering the cantilever.

Finally, we etch the membrane on the lower wafer by using RIE from the back side. The structures at this stage are held by thin silicon beams to the wafer frame. Fig. 3.7 shows a scanning electron micrograph of a finished device with parallel capacitive microlevers. A close-up of the front part of one of the levers is shown in Fig. 3.8. They can easily be removed from the wafer for mounting and wire bonding onto a PCB carrier.

Due to the nature of the etch processes, it is not possible to predict very precisely the cantilever thickness t, which, however, is an important parameter for predicting the mechanical behavior of the device (e.g. k, f, V_t). Unfortunately it is not very accurate neither to determine t with a scanning electron microscope after the lever is free standing.

But since we have good control over the lateral dimensions of the levers (lithographically defined), we can deduce the thickness if the resonance frequency is known. Using the equations (1.1) and (1.2) we find that

$$t \cong \frac{f_0 \, l^2}{1.4 \times 10^3} \tag{3.27}$$

We measured with an interferometer the resonance frequency of several devices with known length l. Table 3.2 shows the result and compares the expected theoretical data with the experimental values of the fabricated devices.

The described technique of the aligned wafer bonding is also interesting for other microfabricated devices. It allows in particular to combine bulk silicon structures with different shapes fabricated by incompatible etch processes, that can be performed on the different sides of the wafer and followed by a bonding step. Other devices like, for instance, micro-optical elements such as torsional mirror arrays and light shutters have been developed using the described technique by Jaecklin and coworkers in our group[16].

Table 3.2 *Comparison of designed and measured values for the thickness and the corresponding resonant frequency of typical capacitive microlevers*

capacitive lever	length l [µm]	thickness t (design) [µm]	res. f_o (design) [kHz]	res. f_o (meas.) [kHz]	thickness t (deduced) [µm]
1	140	3.0	213.9	***210.4***	***3.33***
2	325	3.0	39.7	***39.9***	***3.01***
3	425	3.0	23.2	***25.8***	***2.95***

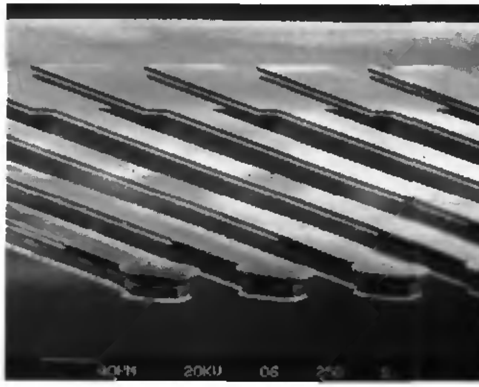

Fig. 3.7: Scanning electron micrograph of an array of microfabricated capacitive cantilevers.

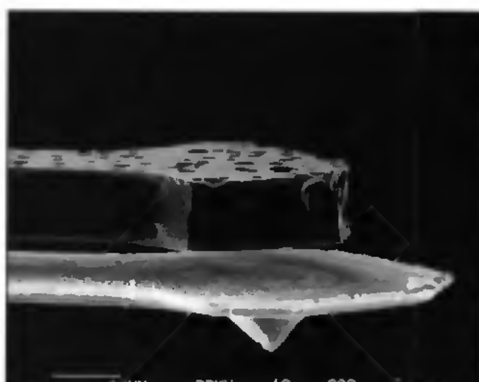

Fig. 3.8: Close-up of a scanning electron micrograph of a microfabricated capacitive cantilevers with integrated tip.

3.5 Experimental results

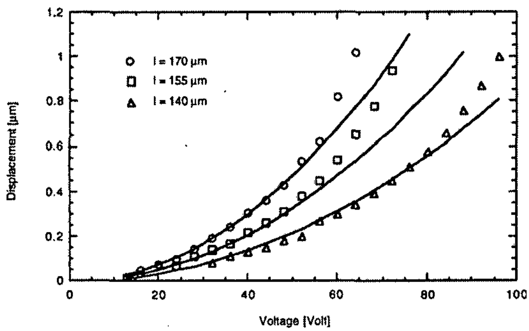

Fig. 3.9: Static deflection curve of a microlever as a function of the applied dc bias voltage. The measured values (confocal microscope) and the theoretical curve (t = 2.8 µm, d = 2.8 µm) are presented.

The microfabricated devices were encapsulated and wire-bonded for experimental characterization. A total capacitance of ≅ 3 pF between the connection pads has been measured. When applying bias voltages the cantilever motion has been measured with an optical confocal microscope or with an interferometer and a phase-sensitive detection (lock-in-amplifier).

Fig. 3.9 shows both the measured and fitted *static deflections* of three cantilevers as a function of the applied dc voltage. The measured values show the expected V^2 behavior and are, for small deflections, in good agreement with the theoretical curve of equation (3.6). For the fitted curve we have assumed a cantilever thickness of t = 2.8 µm and a capacitance gap of d = 2.8 µm, which is consistent with the SEM observations.

Fig. 3.10 and Fig. 3.11 show the measured amplitude of the *dynamic deflection* or vibration for one cantilever with l = 325 µm, w = 40 µm and t ≅ 3 µm, when the frequency of the harmonic excitation voltage of 200 mV (peak-to-peak) is swept from 25 kHz to 45 kHz.

The measurements were performed first in air and then under vacuum condition (0.02 mbar). The measured resonance frequency lies close to 40 kHz. If we define Δf as the full bandwidth at 0.707 of the maximum amplitude, we find a quality factor of $Q = f_0/\Delta f = 15$ in air, and Q = 2000 under vacuum. Due to the small gap between the cantilever and the adjacent counter-electrode damping in air is particularly important for this type of structure. This explains the rather low quality factor observed in air compared to plain silicon cantilever of similar dimensions having Q-factors up to a several hundred in air. When operating the device under vacuum conditions this effects becomes less noticeable.

Also, as predicted by the equations (3.14) and (3.15) the electrostatic field between the cantilever and the counter-electrode leads to a lowering of both, the resonant frequency f_0 and the effective cantilever compliance k'. Fig. 3.12 shows the variation in resonant frequency as a function of the applied DC bias for two cantilevers. The measured data are in good agreement with the computed curves (solid lines) with threshold voltages $V_t = 45$ V and 28 V respectively.

Experimental data using an impedance analyzer have shown that in order to get a sufficiently high current displacement through the capacitor the gap has to be decreased to ≅ 1 µm. Only then the current signal is large enough to be further amplified and fed to the FM detection.

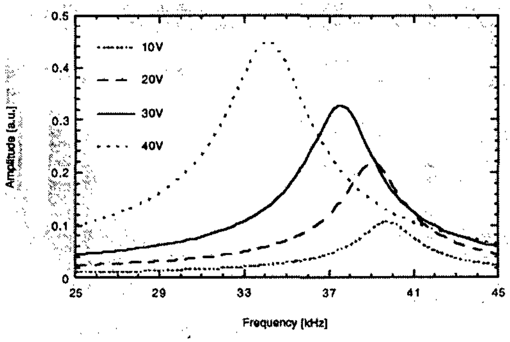

Fig. 3.10: Measured resonance curves of an electrostatically actuated cantilever for various dc bias (V_{dc} = 10, 20, 30, 40 V) and an excitation voltage of 200 mV peak-to-peak. The cantilever dimensions are l = 325 μm, w = 40 μm, t ≅ 3 μm. Measured in air. Q-factor ≅ 15.

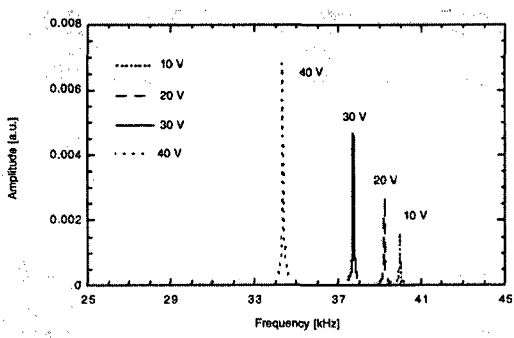

Fig. 3.11: Measured resonance curves of the same structure as in Fig. 3.10 with same voltages, measured under vacuum condition (0.02 mbar). Factor Q ≅ 2000.

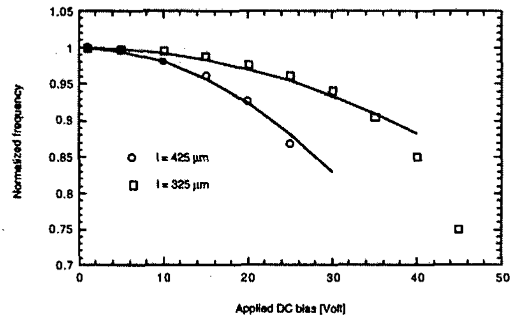

Fig. 3.12: Variation in resonant frequency as a function of the applied dc bias for two cantilevers of length l = 325 µm and 425 µm. The solid lines are computed with V_t = 45 and 28 V respectively.

3.6 SFM in the dynamic mode using microfabricated capacitive sensors

This paragraph summarizes the final results obtained with the microfabricated capacitive cantilevers. The experiments were performed by Nicolas Blanc and Urs Duerig at the IBM Research Laboratory in Rueschlikon. The following passage is an excerpt of a report to be published in J. Vac. Sci. and Technol. B March/April 1996.

Scanning Force Microscopy in the dynamic mode using microfabricated capacitive sensors

We report on the first successful operation of a scanning force microscope using microfabricated capacitive force sensors. The sensors which are made from single crystal Silicon on Insulator (SOI) wafers consist of a cantilever spring with integrated tip at the free end and an electrically insulated counter-electrode. Dynamic force gradient sensing is the preferred operating mode. Here, tip-sample interactions are detected by letting the sensor act as a resonator in a phase controlled oscillator set-up and measuring corresponding shifts of the oscillation frequency. Experiments were performed in vacuum using a standard tunneling microscope. A Cr grating on a quartz substrate served as test sample. Topographic images showing details on a 10 nm scale were obtained operating at a constant force gradient of the order of 0.01 N/m. In addition, critical design parameters are discussed based on an analysis of the electro-mechanical properties of the sensors.

I. INTRODUCTION

The prospects for making miniaturized stand-alone scanning force microscopes has triggered the development of various force sensors with integrated detection schemes such as piezoresistive[a] or piezoelectric cantilevers[b,c]. Compared to optical detection these sensors have a much smaller overall size and do not require any critical alignment of external components. Capacitive detection is also an interesting and very sensitive technique which is commonly applied in the field of pressure sensors and accelerometers. A major advantage of capacitive detectors is the fact that they contain only reactive components and therefore they are free of parasitic resistive noise sources that adversely affect the sensitivity. In the field of Scanning Force Microscopy (SFM) various groups have already reported interesting results based on assembled capacitive set-ups[d,e]. In this paper we present capacitive sensors manufactured by batch processing techniques. Each sensor combines an integrated capacitive detection of the cantilever displacement as well as an electrostatic actuation[f,g,h]. This property makes capacitive sensors particularly attractive for applications requiring parallel operation of large sensor arrays, e.g. as is envisioned in high density data storage devices based on local probe techniques. The fabrication process of these novel devices is based on bulk silicon micromachining of SOI wafers. The electro-mechanical characteristics of the capacitive microlevers are discussed and topographic images of a chrome grating are presented which were obtained in a dynamic operating mode regulating on a constant force gradient.

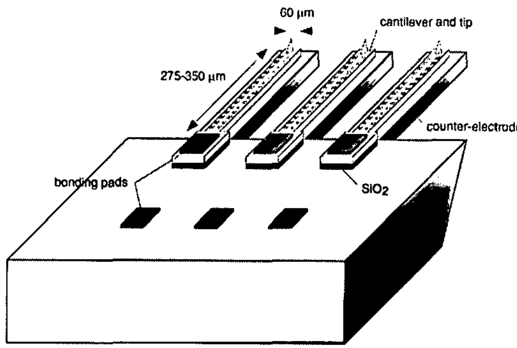

Fig. 3.13: Schematic outline of the capacitive sensor for scanning force microscopy. The cantilever and its counter-electrode are separated by a small gap, typically 1 µm wide, and they are attached to a Si holder containing bonding pads for electrical contacts to the lever and the counter-electrode.

The design of the sensors is schematically shown in Fig. 3.13. They consist of two adjacent, highly doped single-crystal silicon beams forming the two plates of a capacitor. One of the beams, called cantilever (CB), is fairly soft and it serves as spring for sensing interaction forces. A tip is located at the free end of the CB. Typical CB dimensions are: width w = 60 µm, thickness t = 5-6 µm, and length l ranging from 275 µm to 350 µm. The second beam, termed counter-electrode, is essentially rigid and its typical dimensions are: w = 80 µm, t = 15 µm, and l is in the same range as the corresponding CB. The cantilever spring constant and resonant frequency are computed according to

$$k = \frac{3EI}{l^3} \tag{1}$$

and

$$f = 0.162t/l^2(E/\rho)^{1/2}, \tag{2}$$

with $I=wt^3/l^2$ the moment of inertia, $E=1.7*10^{11}$ N/m^2 Young's modulus and $\rho=2300$ kg/m^3 the density of silicon. The spring constant and resonant frequency range from 7 to 26.5 N/m and 57 to 111 kHz respectively. Note that holes have been patterned into the cantilevers in order to promote etching of the thin silicon dioxide layer in the fabrication of the gap between the cantilever and counter-electrode. As a result of the holes, the resonance frequency and the spring constant of the sensors are somewhat smaller than the corresponding values computed by means of equations (1) and (2). The tip can be actuated electrostatically as described in ref. 8. For low applied voltages V the displacement is

$$z_o = \frac{1}{16} \varepsilon_o \frac{V^2}{d^2} \frac{w l^4}{EI} \tag{3}$$

with $\varepsilon_o = 8.85 \cdot 10^{-12}$ As/Vm the permittivity in vacuum and d = 1 μm the gap between the cantilever and counter-electrode. Equation (3) can be written as $z_o = \alpha V^2$ and for the present cantilever dimensions one obtains an α value of the order of 1 nm/V^2.

The devices are fabricated by silicon bulk micromachining. The process is illustrated in Fig. 3.14. Silicon on insulator (SOI) wafers with a 15 μm thick n-type (100) oriented silicon film, a 1 μm thick buried SiO_2 layer and a 400 μm thick n-type (100) oriented silicon substrate were used). The resistivity of the Si was of the order of 10 Ohm cm which turned out to be somewhat high for sensor applications (see below). Silicon dioxide is first thermally grown to a thickness of 1.7 μm on both sides. Three photolithographic and subsequent SiO_2 etching steps in buffered hydrofluoric acid (BHF) are used to pattern the oxide mask and define the cantilevers and tips as well as the backside etch windows. The counter-electrode is etched by reactive ion etching (RIE) with photoresist as a mask. The buried oxide spacer layer between the CB and the counter electrode is then removed by BHF etching and the photoresist is stripped in acetone. The cantilevers with integrated tips are defined by successive RIE and BHF etchings as previously reported for simple cantilevers[i]. In order to lower the resistivity of the cantilever structure a phosphorus-doped silicate glass (PSG) is deposited, followed by a diffusion step and the removal of the PSG layer in BHF.

A 1 μm thick layer of aluminum is then deposited, patterned and alloyed for 30' at 450 °C to form the ohmic contacts to the cantilevers and the substrate. A membrane, typically 30 μm thick is defined by anisotropic etching in KOH from the backside while protecting the top side in a mechanical chuck. An appropriately patterned photoresist cover layer protects the aluminum bonding pads from being attacked in the subsequent fabrication steps. The counter-electrodes and the cantilevers are released by RIE from the backside and BHF etching respectively. Finally the resist is stripped and the cantilevers bonded. Fig. 3.15 shows micrographs of the microfabricated capacitive cantilevers after the completion of the process.

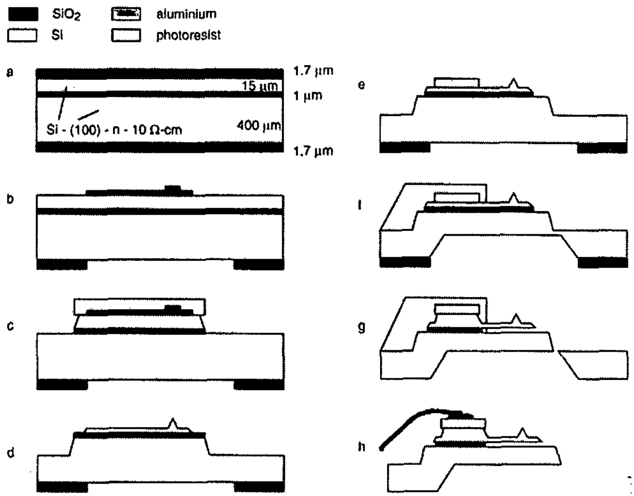

Fig. 3.14: Process steps in the microfabrication of the capacitive microlevers.

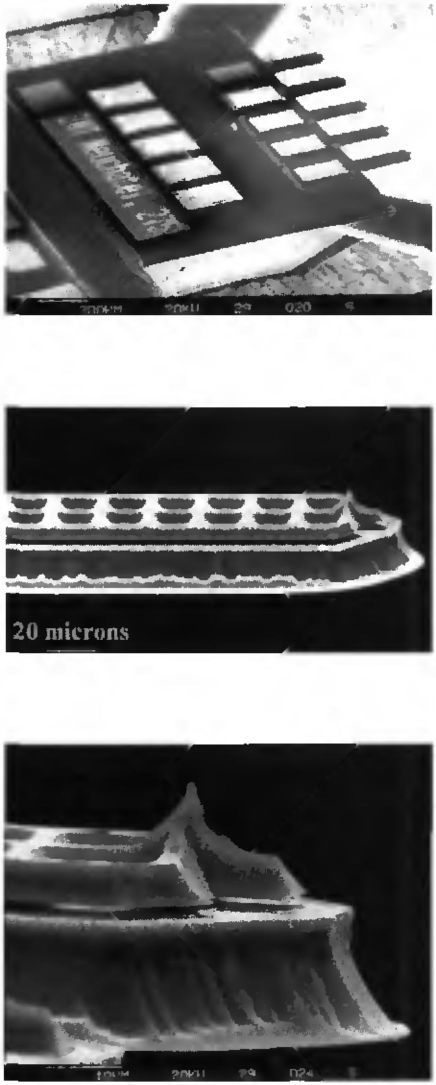

Fig. 3.15: top: SEM micrographs of micromachined capacitive cantilever sensors.; area (tip), enlarged views of the end section of the lever showing the integrated probe tip (center, bottom)

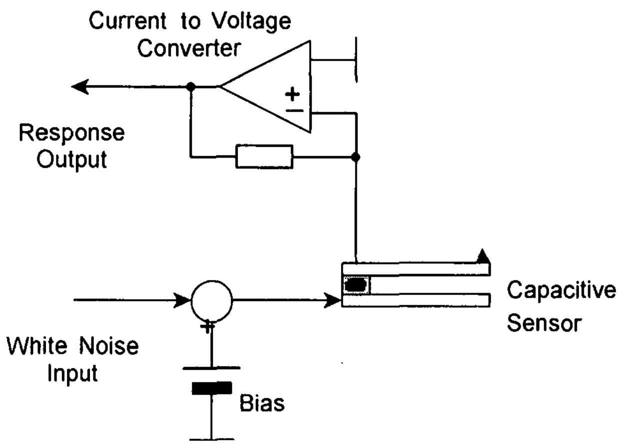

Fig. 3.16: Schematic diagram of the set-up used in the admittance measurement. Note that the CB is virtually grounded by means of the current to voltage converter and hence the effect of stray capacitances is minimized.

The frequency response of the electrical impedance of the capacitive sensor deviates significantly from the one of a simple capacitor due to the coupling of the mechanical motion of the CB and corresponding electrical fields. The frequency response can be modeled by the same equivalent circuit that applies to a quartz crystal resonator. It consists of a series resonant circuit which is shunted by a capacitance[j]. A detailed analysis shows[k] that observability of the resonant properties and the overall performance of the capacitive sensor can be expressed in terms of a single parameter that is to be maximized and which scales as the square of the applied biasing voltage and the inverse cube of the gap width between CB and counter electrode. Hence, the quality of the insulating oxide layer and of the capacitor gap are crucial for successful operation of capacitive sensors.

For practical reasons the admittance which is the inverse of the impedance was measured using a spectrum analyzer (Fig. 3.16). For this purpose a small (of the order of 5 mV) white noise driving voltage[g,h] superimposed on a DC bias voltage (36 V in the example shown) is applied. The current that is induced in the capacitive sensor is measured by means of a virtual ground type current to voltage converter. By this scheme the electrical potential of the cantilever (and the tip) is clamped to ground potential thereby virtually suppressing effects due to unavoidable stray capacitances. This point is somewhat critical as the capacitance of the lever is only of the order 0.1 pF. The frequency response of admittance measured on a cantilever with a length of 300 μm is shown in Fig. 3.17. Series and parallel resonance can be clearly identified at f_S = 60'147.5 Hz and f_P = 60'217.5 Hz, respectively. As expected a sharp transition in the phase response is observed. The phase shift amounts to 160° and the slope measured at the series resonance is $\delta\phi/\delta f)_{f=f_S}$ = 9°/Hz from which a quality factor of the resonance of the order of $Q = f/2\ \delta\phi/\delta f)_{f=f_S}$ = 4'700 can be deduced. The observed Q-factor appears to be somewhat low. The reason for this is the high value of the specific resistance of the Si wafers used. The Q-factor is lowered because of resistive dissipation induced by the motion of space charge at the surface of the CB and the counter-electrode when the electric field is being modulated by the vibration of the CB. Quality factors as high as 50'000 have been obtained in test devices that were doped close to the limit of degeneracy.

With increasing applied DC voltage the resonant frequency decreases as shown in Fig. 3.18. This corresponds to a lowering of the effective cantilever spring constant. At low applied DC bias the frequency shift is proportional to the voltage squared. From this data the mechanical resonant frequency (at V_{dc} = 0) is extrapolated to be 66'585 Hz. The physical dimensions of the cantilevers were checked by scanning electron microscopy. The observed thickness of the levers varied between 5 and 6 μm. From equation (2) we compute a resonance frequency in the range 77-93 kHz for cantilevers with a length of 300 μm. These values are higher than the experimentally determined resonance frequency. This difference is attributed to the effect of the holes in the cantilever. Note that due to thickness variation the measured resonance frequency itself also varies by a substantial amount. Values as high as 85 kHz have been observed for the type of cantilcvers used in the experiments.

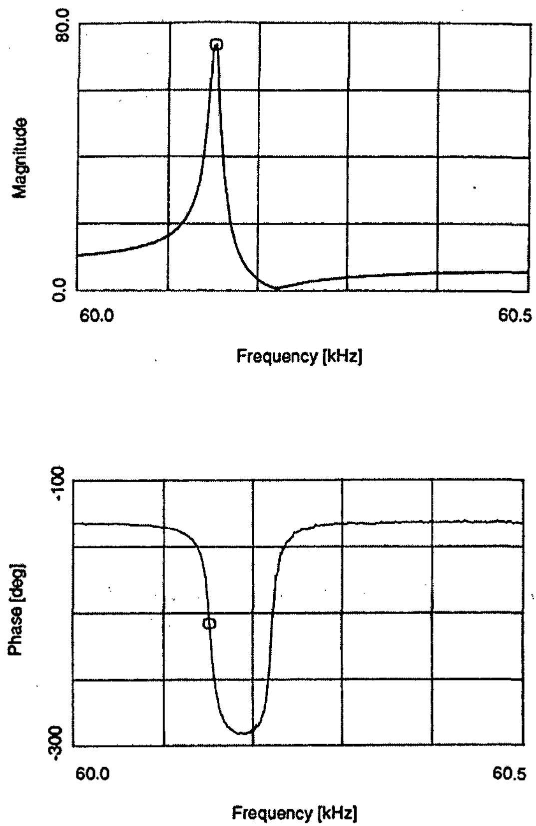

Fig.3.17: Measured frequency response (admittance amplitude and phase) of a capacitive cantilever with a length of 300 μm. The applied bias is V_{dc} = 36 V.

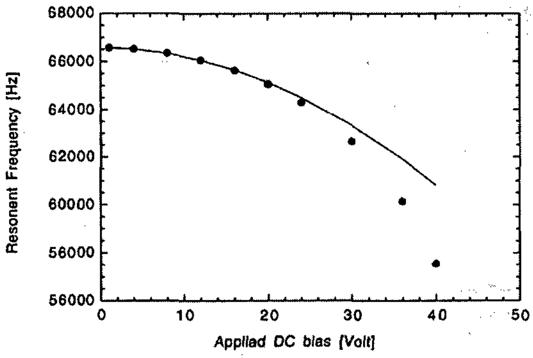

Fig. 3.18: Measured series resonant frequency as a function of applied DC bias for a cantilever with a length of 300 μm. The solid line corresponds to $f_s = 66'585 - 3.6\ V_{dc}^2$

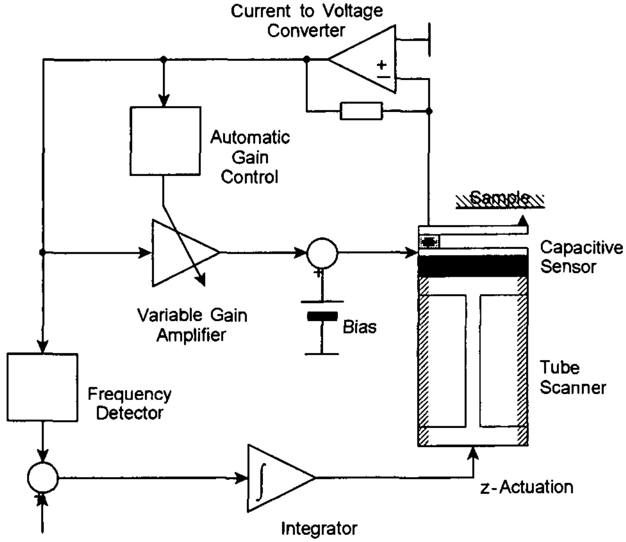

Fig. 3.19: Schematic diagram of the oscillator and the associated feedback control loop which controls the tip-sample distance by regulating on a constant frequency shift.

Dynamic force gradient sensing is the preferred operating mode for capacitive force sensors. The method exploits the fact that the resonance frequency of the CB shifts according to the interaction force gradient acting between the tip and the sample. Implementation of the scheme is straightforward as the capacitive sensor acts like a resonant electrical two-terminal device. For measuring the resonance frequency a set-up similar to the one used for the admittance measurement was employed (fig. 3.19). The sensor serves as the frequency determining element (operating at series resonance) in an oscillator circuit which consists of a variable gain feedback amplifier and an automatic gain control to maintain a constant vibration amplitude[12]. The oscillation frequency is measured by means of a phase-locked-loop frequency detector which has a bandwidth of 10 kHz.

Experiments were performed in vacuum in order to avoid damping of the CB oscillation by the ambient air. A DC bias of 10 V was applied and an AC driving voltage of the order of 5 mV was sufficient to induce a vibration amplitude of 50 nm at the free end of the cantilever. A Cr grating on a quartz substrate was used as test sample. The pitch of the grating was 250 nm and the Cr lines had a height of 100 nm. Topographic imaging was performed in a constant force gradient operating mode meaning that the feedback loop controlling the tip-sample distance was regulating on a constant frequency shift. At these conditions the noise of the output of the frequency detector was of the order of 2 Hz measured over a bandwidth of 1 kHz. This noise level is roughly a factor two larger than the fundamental thermal oscillator noise limit[1]. A positive shift of 50 Hz was selected as imaging parameter in Fig. 3.20) showing a 1.5 μm x 1.5 μm section of the grating. The frequency shift translates into a positive interaction force gradient of the order of 0.01 N/m (assuming a spring constant of 10 N/m) meaning that the overall tip-sample interaction was repulsive. In fact, operation of the force microscope is better described in terms of a high frequency tapping mode given that the vibration amplitude of the CB was of the order of 50 nm. In each oscillation cycle the tip pushes against the sample for a short fraction of the oscillation period. The repulsive force that was exerted by the tip during touching can be estimated to be of the order of 500 pN assuming 1 nm for the range of interaction. The drive voltage necessary to maintain a constant amplitude of vibration is a measure for dissipation[1]. By monitoring this voltage (see Fig. 3.20), one can thus obtain information on local variations of dissipative channels of the tip-sample interaction. Correlation of the topography with corresponding variations of the damping factor can easily be recognized. Damping forces are highest when the tip is following a trench between Cr lines and they are smallest when the tip is on top of a Cr line. At this point we lack a firm understanding of the physical mechanism that is causing this variation of the dissipative interaction. From the correlation with the topography, namely dissipation being minimum on top of the protrusions and maximum at the edges of the ridges, one might speculate that the dissipation is caused by frictional forces as the tip is touching the sample surface.

To conclude we have shown that microfabricated capacitive sensors can be used for scanning force microscopy in the dynamic mode. With this device the experimental set-up can be greatly simplified with respect to many of the conventional schemes: No optical components for the tip displacement sensing are needed, and moreover, as shown in this paper the integrated electrostatic actuation can be used to excite the levers at resonance meaning that no additional actuators are required. Static actuation is also conceivable. However, one must keep in mind that the electrostatic potential applied to the actuator also influences its resonance frequency. Therefore, compensation schemes are needed in order to separate this effect from genuine interaction induced changes of the resonance frequency.

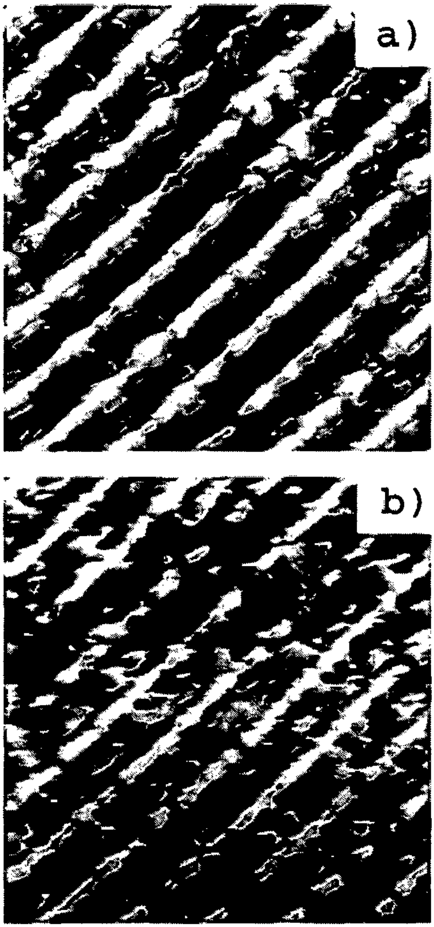

Fig. 3.20: Dynamic force gradient imaging of a Cr grating with a pitch of 250 nm on a quartz substrate. The total scan area is 1.5 μm x 1.5 μm. The image was obtained in the repulsive ("tapping") mode at an effective positive force gradient of 0.01 N/m. a) Topography: Height variation between trenches, shown dark, and ridges, shown bright, corresponds to 80 nm. b) Dissipation: Low and high dissipation are shown as bright and dark tones, respectively. The dissipation in dark areas is about two times stronger than in bright areas.

IV. ACKNOWLEDGMENTS (paper)

The authors wish to thank C. Ketterer and P. Sixt from CSEM for performing the SEM studies and providing the Cr grating respectively. Technical assistance from P.A. Clerc and S. Pochon (IMT), from P. Lacombe and J. -D.Cretin (Microsens) and from T. Mezzacasa (PSI) is gratefully acknowledged. This work was supported by the Swiss National Science Foundation.

V. REFERENCES (paper)

a *M. Tortonese, H. Yamada, R. C. Barrett, and C. F. Quate, Tech. Dig. Int. Conf. Solid-State Sensors and Actuators (Transducers'91), San Fransisco, CA, June 1991, pp. 448-451.*

b *T. Itoh, T. Suga, Digest of technical papers, Transducers'93, Yokohama, Japan, June 1993, pp. 610-613.*

c *S. Akamine, T. R. Albrecht, M. J. Zdeblick and C. F. Quate, Sensors and Actuators, A21, 964 (1990).*

d *T. Goddenhenrich, H. Lemke, U. Hartmann, and C. Heiden, J. Vac. Sci. Technol., A8 (1), 383 (1990).*

e *G. Neubauer, S. R. Cohen, G. M. McClelland, D. Horne, and C. M. Mate, Rev. Sci. Instrum., 61 (9), 2296 (1990).*

f *L.C. Kong, B. G. Orr, and K. D. Wise, J. Vac. Sci. Technol. B 11(3), 634 (1993).*

g *J. Brugger, N. Blanc, Ph. Renaud and N. F. de Rooij, Sensors and Actuators A,43, 339 (1994).*

h *N. Blanc, J. Brugger and N. F. de Rooij, Electrostatically actuated silicon micromachined sensors for scanning force microscopy, Forces in Scanning Probe Methods edited by H.-J. Guntherodt et al., NATO ASI Series E: Applied Sciences Vol. 286, 79-84 (1995).*

i *J. Brugger, R.A. Buser and N. F. de Rooij, Sensors and Actuators A, 34, 193 (1992).*

j *M. W. Putty, M.S. Thesis, University of Michigan at Ann Arbor, 1988*

k *N. Blanc, U. Duerig, to be published*

l *T.R. Albrecht, P. Grutter, D. Horne, and D. Rugar, J. Appl. Phys. 69(2), 668 (1991); U. Duerig, O. Zueger, A. Stalder, J. Appl. Phys. 72(5), 1778 (1992).*

3.7 Conclusions

In this chapter we have presented a capacitive device useful for force detection in scanning force microscopy. We have shown that the device can be microfabricated with a batch process based on single crystal silicon. It allows for the cost effective fabrication of large numbers of devices on a single wafer. The key features of the microlever (i.e. its integrated sensing and actuation functions) have been evaluated analytically and have been compared with the experimental results.

We could show that the cantilever can be actuated via the capacitor by the electrostatic forces in a quasi-static mode for the fine tip-sample distance adjustment. Depending on the lever geometry we could deflect the tip up to 1 µm (!) with a dc bias voltage of ≅ 60 V. This experimental result corresponds well with the theory.

In the dynamic mode the cantilever could be actuated to vibrate at its resonance. The expected change in frequency, and hence of the spring constant, due to a superimposed force is demonstrated and corresponds well with the computed data. This feature allows to tune the cantilever compliance and to operate the sensor in various regimes of attractive forces.

We have shown that the signals that we could obtain with the 3 µm gap devices are too low for high resolution surface imaging. An improved device made by SOI wafer substrates with a capacitive gap of 1 µm could be successfully used for dynamic mode SFM imaging for the first time.

---

[1] R.V. Jones, J.C.S. Richards, Journal of Physics E: Scientific Instruments 1973 Volume 6, 1973, p. 589

[2] W.Chr. Heerens; J. Phys. E: Sci. Instrum. 19 (1986), p. 897

[3] F. Rudolf, A. Jornod, J. Bergqvist, H. Leuthold; Sensors and Actuators, A21 - A 23 (1990), pp. 297-302

[4] G. Binnig, U. Dürig, J.K. Gimzewski, D. Pohl, H. Rohrer, Atomic force sensor head, Eur. Patent Appl. EP-A 0 290 648 (May 12, 1987)

[5] T. Göddenhenrich, H. Lemke, U. Hartmann, C. Heiden, J. Vac. Sci. Tehcnol., A8 (1) 1990, pp. 383-387

[6] G. Neubauer, S.R. Cohen, G.M. McClelland, D. Horne, C.M. Mate, Rev. Sci. Instrum., 61 (9), 1990, pp. 2296-2308

[7]. H.C. Nathanson, W.E. Newell, R.A. Wickstrom, J.R. Davis; IEEE Transactions on Electron Devices, Vol. ED-14, No. 3, March 1967

[8] R.J. Roark, W.C. Young, Formulas for stress and strain, McGraw-Hill, Singapore, 5th edn., 1976, ch.7

[9] C. Linder, Dissertation, University of Neuchâtel, 1993

[10] S. Timoshenko, D.H. Young, W. Weaver; 'Vibration problems in engineering', Wiley, New York, 4th edn., 1974, pp. 72

[11] T. Albrecht, P. Grütter, D. Horne, D. Rugar; J. Appl. Phys. 69 (2), 15 January 1991, p. 668

[12] K. Petersen, P. Barth, J. Poydock, J. Brown, J. Mallon, J. Bryzek; Technical Digest of the IEEE Solid-State Sensor and Actuator Workshop, Hilton Head Island, SC, June 6-8, 1988, p. 145

[13] e.g. Ch. Harendt, B. Höfflinger, H.-G. Graf, E. Penteker; Sensors and Actuators A, 25-27 (1991) 87-92

[14] AL6-2 by Electronic Vision Company, Austria

[15] R.W. Bower, M.S. Ismail, S.N. Farrens; J. of Electronic Materials, Vol. 20, No. 5, 1991, p. 383

[16] V. Jaecklin, Dissertation University of Neuchâtel, 1993

1296

Chapter 4
Piezoresistive microlever

In the previous chapter we described a capacitive device to detect and induce cantilever motion. In this chapter we discuss a piezoresistive cantilever deflection sensor.

Piezoresistivity is the material constant that describes the change of the bulk resistivity as a function of the mechanical stress applied to the material. The use of the piezoresistive effect for micromechanical sensors is not new. In particular in the last decade pressure sensors and accelerometers became well studied devices[1,2] and established industrial products.

In 1991 Tortonese and co-workers at Stanford University demonstrated the feasibility of using a piezoresistive cantilever deflection sensor for SFM applications[3]. The contribution here follows a similar concept and includes the novelty of confining the piezoresistor to specific areas on the cantilever. This increases the sensitivity and, in particular it enables lateral force measurements in our chosen layout. We also demonstrate the feasibility of using a piezoresistive lever array for simultaneous parallel surface imaging.

The device described in this chapter has been designed and fabricated during a 1 year visiting research period at the Advanced Research Laboratory, HITACHI Ltd. in Kokubunji-shi.

4.1 Design and analysis

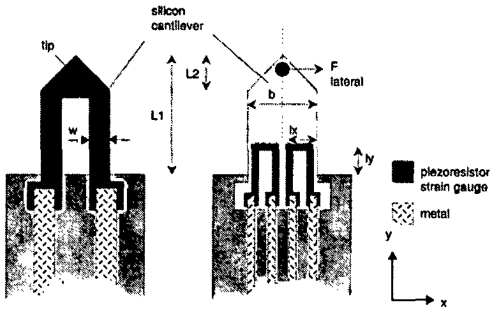

Fig. 4.1: Schematic layout of the piezoresistive microlevers described in this work; U-shaped cantilever for bending (a), and PR-loop type lever for torsion measurement (b)

The heart of the device consists of a silicon cantilever beam with an integrated tip and with a piezoresistive strain gauge. A load applied at the tip deflects the cantilever and the resulting stress in the material induces a change of the resistivity. This effect can be measured by appropriately guiding a current through the stressed regions of the cantilever. We can do this in two ways. Tortonese and co-workers have proposed an uniformly doped *U-shape cantilever* (Fig. 4.1a) where the current enters in one leg and exits through the other. In our new version (Fig. 4.1b) the *piezoresistor loops* are defined by an additional photolithography step near the cantilever base. The stress has a maximum at this location and we expect an increase of the device sensitivity. Furthermore, if the piezoresistors are symetrically arranged to the central axis of the lever, the device becomes sensitive to cantilever torsion, and, hence can be used for sensing lateral forces, e.g. in a friction force microscope.

The lateral dimensions of the piezoresistive microlevers are precisely defined by means of lithographic processes. Table 4.1 summarizes the geometrical dimensions. The lever thickness is fixed for a given wafer and is defined by the micromachining etching process. We aimed at a lever thickness between 2 and 5 μm. The corresponding spring constant k and the resonant frequency f are summarized in Table 4.2. For the calculation in the case of the

U-shaped device, we approximated the double-beam lever by a plain lever with twice the width W.

Table 4.1 *Geometrical dimensions of piezoresistive microlevers*

ID #	Type	L_1 [µm]	L_2 [µm]	W [µm]	B [µm]	l_y [µm]	l_x [µm]
1	U-shape	100	35	20	55	75	55
2	U-shape	125	45	25	65	80	65
3	U-shape	280	80	40	95	200	95
4	U-shape	420	80	50	130	340	130
5	loop	325	80	-	100	140	30

Table 4.2 *Calculated spring constant and resonant frequency for various cantilever thickness t*

ID #	t = 2 μm		t = 3 μm		t = 4 μm		t = 5 μm	
	k [N/m]	f [kHz]	k [N/m]	f [kHz]	k [N/m]	f [kHz]	k [N/m]	f [kHz]
1	13.5	277	45	415	108	555	210	693
2	8.6	177	29	266	69	355	134	444
3	1.0	35	4.0	53	10	71	19	88
4	0.5	16	1.5	24	3.6	31	7.1	39
5	0.9	26	3.3	39	7.9	52	15	66

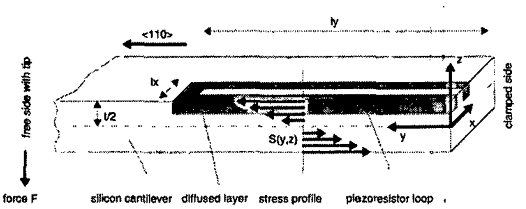

Fig. 4.2: Cantilever model for analytical calculation showing a cantilever portion with the diffused layer profile and the coordinate axis and the stress profile due to bending.

The non deflected cantilever has a resistance value of $R = \rho\ l/A$ which is given by the resistivity ρ of the conducting layer, the length l and the cross section A of the current path. We want to calculate the fractional change of resistance ÆR/R due to a bending Æz of the cantilever end. For this we need to determine a relationship between the mechanical stress and the resultant resistivity change. The coordinate axis for the mathematical expressions are defined as shown in Fig. 4.2.

A deflection Δz at the tip of the cantilever creates a torque M along the cantilever which is a function of the applied force F and the distance y from the fixture.

$$M(y) = F\,(y - L_1)$$

$$= k\,\Delta z\,(y - L_1) \qquad (4.1)$$

L_1 is the cantilever length and k is the spring constant. M(y) is maximum for y = 0, which is at the basement of the cantilever. The induced stress S(y) in the cantilever is a function of the couple M(y) and the distance z from the neutral line in the cantilever

$$S(y,z) = \frac{M(y)}{I}\,z \qquad (4.2)$$

where I is the cross sectional moment of inertia of the cantilever beam. For high sensitivity it is important to place the piezoresistor at the surface, i.e. at $z = \pm\, t/2$ where the stress is maximal. In a fabrication process this can be realized by means of a diffusion or an ion implantation process. At the surface the stress is then given by

$$S(y,t/2) = \frac{M(y)\,t}{2\,I} \tag{4.3}$$

The relative change in resistivity of silicon under stress is a function of the piezoresistive coefficient π and the stress.

$$\frac{\Delta\rho}{\rho}(x,y,z) = \pi\, S(y,z)$$

$$= \frac{\pi\, k\, t}{2\, I}\,(y - L_1)\;\Delta z \tag{4.3}$$

By integrating the above expression over the path L_p that the signal current has to take through the piezoresistors we obtain the general expression for the fractional change of resistance.

$$\frac{\Delta R}{R} = \frac{1}{L_p}\int_0^{L_p} \frac{\Delta\rho}{\rho}(y)\; dl$$

$$= \frac{1}{L_p}\,\frac{\pi\, k\, t}{2\, I}\;\Delta z \int_0^{L_p} (y - L_1)\, dl \tag{4.4}$$

When replacing k and I we find

$$\frac{\Delta R}{R} = \frac{4}{3}\,\frac{\pi\, E\, t}{L_1{}^3}\,\Delta z \int_0^{L_p} (y - L_1)\, dl \tag{4.5}$$

Equation (4.5) shows that the basic sensitivity for a piezoresistive microlever with a given spring constant k and a cross sectional moment of inertia I increases for a thicker and shorter cantilever, weighted by the integration over the current path along the legs.

The piezoresistive coefficient π depends on the crystal orientation[4]. For (100) silicon wafer substrates the longitudinal coefficient π_L has a maximum value in the <110> crystal direction. This, and fabrication related issues are the reasons why our cantilevers point in that direction. For these substrates we also find that the longitudinal and the transversal coefficient are of same magnitude but with opposite sign, i.e. $\pi_L = -\,\pi_T$. Thus, each portion of the piezoresistor which is directed transversally to the deflected cantilever beam decreases the sensitivity.

Assume l_y and l_x being the length of a portion of the piezoresistor pointing into the longitudinal axis y and the transversal axis x, respectively. Integrating equation (4.5) yields the general expressions for the fractional resistance change in the y and x direction:

$$\left(\frac{\Delta R}{R}\right)_y = \frac{4}{3}\frac{\pi_l E t}{L_1^3}\left(\frac{l_y}{2} - L_1\right) \Delta z \qquad (4.6a)$$

$$\left(\frac{\Delta R}{R}\right)_x = \frac{4}{3}\frac{\pi_t E t}{L_1^3}(l_y - L_1) \Delta z \qquad (4.6b)$$

The longitudinal contribution $(\Delta R/R)_y$ is averaged over the length of l_y, i.e. it corresponds to the value obtained at the location $y = l_y/2$. This makes sense because the couple M(y) and hence the stress S(y) decrease linearly along the cantilever. The contribution of the transversal contribution $(\Delta R/R)_x$ can be calculated accordingly by taking the constant value of the stress at the location $y = l_y$.

For high sensitivity according to the above equations we have to make l_y short and place it as close as possible to the lever base in order to have a high average stress in the piezoresistor. On the other hand we have to minimize l_x and place it as far away as possible from the base.

For the *U-shaped* cantilever the location of l_x is fixed on the triangular portion that connects the two legs. Tortonese et al. have shown for this case that it has negligible effect on the change in resistance due to bending, because in this region far away from the base the stress is much smaller than in the legs.

In the case of the *piezoresistor loop* type, the location of l_x can be defined by means of a lithographic process (see Fig. 4.1). In our present design, we have chosen $l_y = L_1/2$, and $l_x = 0.2\, l_y$. A calculation shows that for this case the loss in sensitivity due to l_x is less than 10 %. In order to further increase the sensitivity of the device in a future design a metal line could be used to short circuit the undesired piezoresistor portion in l_x.

For our cantilevers we obtain calculated sensitivities ΔR/R per Å deflection in the range of 1×10^{-6} and 1×10^{-7} for the shorter and longer cantilevers, respectively. A summary of the calculated sensitivity for the different cantilever dimensions can be found in Table 4.3.

So far we have assumed that the piezoresistors are located at the cantilever surface. In practice this is not true and the doping concentration has a specific profile given by the implantation process. In diffused or implanted layers the impurity concentration decreases with depth. It is known that the coefficient π decreases with increasing impurity concentration[5], and hence the piezoresistive coefficient shows an increasing profile with depth. The local coefficient $\pi(z)$ has to be weighted by the conductivity $\sigma(z)$, which is, again, a function of the doping profile. In general we can express the effective piezoresistive coefficient by

$$\pi_{eff} = \frac{\int_0^j \pi(z)\sigma(z)dz}{\int_0^j \sigma(z)dz} \qquad (4.7)$$

where j is the junction depth (≅ 0.3 μm in our case). The ratio $\beta = \pi_{eff}/\pi$ is a number between 0 and 1. When $\beta = 1$, then the doped layer is at the surface, and when $\beta = 0$, the cantilever is uniformly doped. In the latter case the sensitivity $\Delta R/R$ drops to zero since opposite stresses in the cantilever cross section cancel each other out. A typical value of β valuc is 0.8 for our process. It depends mainly on the implantation depth and the cantilever thickness.

Noise in the piezoresistive microlever

The minimum detectable deflection of the cantilever does not only depend on the sensitivity of the measurement system but also on the noise. The noise arises from several sources: the thermal mechanical noise of the cantilever, the noise in the resistors and the amplifier noise.

The thermal mechanical noise of a free standing cantilever in the vertical degree of freedom is given by $\Delta z_n = \sqrt{k_B\, T\, k^{-1}}$, where k_B is the Boltzmann constant ($k = 1.38 \times 10^{-23}$ J/K), T is the absolute temperature and k is the spring constant. For a typical cantilever with a spring constant of 1 N/m we obtain $\Delta z_n = 0.6$ Å. For contact mode imaging this noise becomes irrelevant since the cantilever tip is in contact with the surface and looses this degree of free vibration.

The thermal or Johnson noise in a resistor R is given by $v_n = \sqrt{4\, k_B\, T\, R\, B}$, where B is the frequency bandwidth of the measurement set-up. This is the fundamental limit in the measurement of resistance. The other sources are the noise in the electronics which however can be made negligible at room temperature, and 1/f noise which becomes dominant when operating at high bridge voltages. Tortonese has demonstrated that the best performances are achieved when using piezoresistors with a few kΩ and a bridge bias voltage of 5 to 10 Volt.

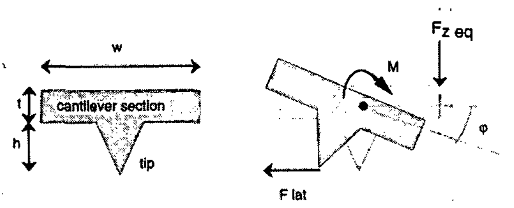

Fig. 4.3: Lateral force F_{lat} on the tip induce a torsion couple M in the cantilever of angle φ.

A lateral force F_{lat} applied on the tip with height h creates a torque $M_{tor} = F_{lat} \times h$ in the lever. We can analyze the response of the torsion sensor by making the assumption that the center of lever rotation lies on its axis. This is not exactly true since the lateral force is applied on the tip at some distance h off the cantilever bottom. Depending on the geometry of the lever it is either the bending or the torsion that is dominant. The lateral spring constant of the lever is given by

$$k_l = \frac{E\,t\,w^3}{4\,L_l} \qquad (4.8)$$

The angle of beam torsion φ is proportional to the torque M and inversely proportional to the torsional rigidity k_t

$$\varphi = \frac{M}{k_t} \qquad (4.9)$$

where k_t is given by the lever material and geometrical constants. According to Colchero and coworkers [6] it can be expressed by

$$k_t = \frac{G\,K\,w\,t^3}{3\,L_l\,h^2} \qquad (4.10)$$

where $G = E/2(1+\sigma)$ denotes the shear modulus and σ the Poisson number of the material. For silicon they amount to 0.7×10^{11} N/m^2 and 0.3 respectively[7]. K is a geometrical factor depending on the ratio w/t of the lever. For w = t (a lever with a square cross section) $K \cong 0.425$, and for w >> t it converges to 1. In our case with typical t = 3 µm and w = 100 µm we obtain $K \cong 0.98$. The ratio between the force constants for lateral bending k_l and for torsion k_t is

$$\frac{k_l}{k_t} \cong 0.5 \left(\frac{h\,w}{t\,L_l} \right)^2 \tag{4.11}$$

Typically, in friction force microscopes the cantilever torsion is monitored, e.g. by an optical beam deflection system using a 4-segment photo diode.

In the case of the piezoresistive microlevers the *loop* cantilever (Fig.4.1b) in contrast to the U-shaped device can be used to sense the torsion of the microlever as a result of the particular arrangement of the resistors on the stressed beam. A twisted lever induces stresses with opposite signs symmetrically along the lever axis. Our measurement uses a differential bridge amplifier that compares the amplitudes of the two output signals ΔR_1 (left loop) and ΔR_2 (right loop). If ΔR_1 equals ΔR_2 then we have pure bending, and if $\Delta R_1 = - \Delta R_2$ we have pure torsion. In most practical cases there will be a combination of both.

By using this devices we can reduce the complexity of the instrument for friction experiments and gain access to multiple probe operation.

4.2 Microfabrication

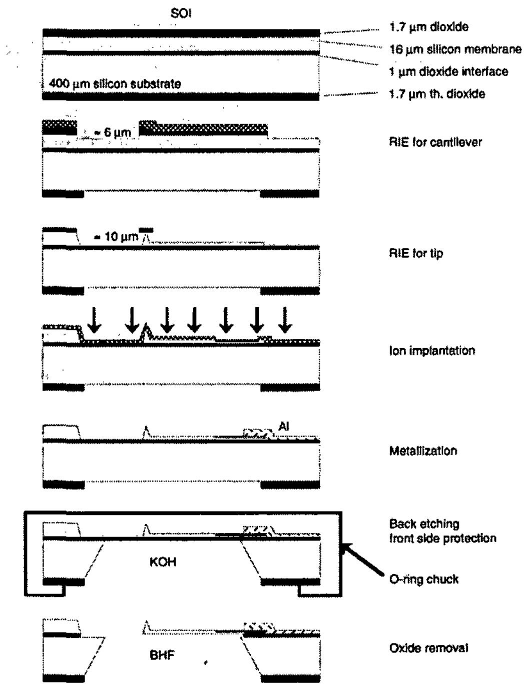

Fig.4.4: Outline of the microfabrication process; for details refer to text.

Silicon-on-insulator (SOI) substrates are used for the fabrication of the piezoresistive sensors. SOI substrates can be purchased by several suppliers. Our 3-inch SOI wafer are custom made by Mitsubishi Materials Inc., Japan. The oxide interface serves as effective etch-stop during the backside etching process and isolates the active probes electrically from the handle piece. The wafers are double side polished and have following layer configuration (from bottom to top): 1.7 µm thermal silicon dioxide, 400 µm silicon carrier wafer, 1 µm dioxide interface, 16 µm silicon membrane and 1.7 µm thermal dioxide.

The complete process flow is depicted in Fig.4.4. The first step is to pattern the top-side oxide to a small cap that will serve later as etch mask for the tip etching (cf. chapter I). Simultaneously the back-side oxide is opened in a double-side process to form the windows for the KOH backside etching. Then a 8 μm thick photoresist layer is applied to the top-side and patterned to the shapes of the cantilevers. With a dry etching step we transfer the resist pattern about 5 - 6 μm into the silicon to form a pre-shape of the cantilever beam. After stripping of the remaining resist the underlying oxide pads become visible again and can be used to etch the tips now. The circular masks have a diameter of 15 μm. The etching is stopped at the SOI oxide interface. All the process parameters are optimized in order to leave nearly finished tips after this etching which can be sharpened with a low temperature oxidation. The present structure is left untouched in place until the very end of the process when a BHF etch removes the dioxide and frees the tips. The dioxide caps and oxide layer protects thereby the tips during all subsequent process steps. Then the piezoresistor are defined by an ion implantation process. Boron is used as doping since p-type resistors yield a higher stress sensitivity, compared to n-type resistors, for the given silicon crystal orientation. The implantation parameters are: doses 1×10^{15} ions/cm^2 and energy 80-120 keV. A doping concentration of 1×10^{19} atoms/cm^3 is chosen for the piezoresistors as a compromise between high piezoresistance coefficient and low temperature coefficient. The resulting sheet resistance is approximately 300 Ω/square yielding an estimated piezoresistance value of a few kΩ for our typical cantilevers.

In the case a confinement of the resistor is required we lithographically pattern beforehand the region for the doping onto the cantilevers. The photoresist is subsequently stripped. An aluminum layer is deposited, patterned and etched for the contacts to the wire bond pads. At this point the top-side processing is finished and before the back-etching is performed we should measure some device parameters such as the cantilever thicknesses for instance. This will help us to estimate the mechanical characteristics. Fig. 4.5 shows a map of one of our wafers with 15 chips and their corresponding cantilever thicknesses. You can see that there is a significant variation in thickness from chip to chip. One possible origin can be the variation of the initial membrane thickness of the SOI substrate (supplier specification is ± 1 μm). Another possible effect can occur during the dry etching process with non uniform cantilever thickness at different locations on the wafer. There is a noticeable circular decreasing gradient of the etch rate from the wafer center (5 μm) to the border (≅ 3 μm).

Finally the wafer is etched back in a KOH solution while the top-side is protected in a mechanical O-ring chuck. The etching stops at the SOI interface layer which is then removed in BHF solution. In order to protect the aluminum the BHF is modified with glycerin[8]. Fig. 4.6 and 4.7 show SEM micro graphs of finished devices. They are encapsulated and wire bonded to sample holders as shown in Fig. 4.8.

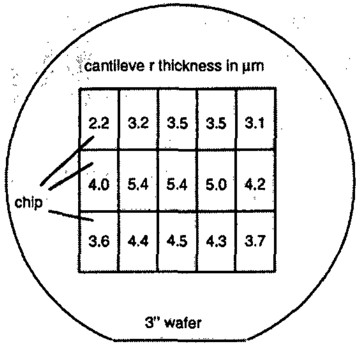

Fig. 4.5: Wafer map showing the measured cantilever thickness variations on a single wafer. The thickness decreases in a circular gradient from a maximum in the center (5.4 µm) to a minimum in one corner near the border (2.3 µm).

Fig. 4.6: Scanning electron micrograph of two microfabricated piezoresistive microlever in U-shape. At the front part the integrated tip can be seen. The aluminum metal connection can be seen at the upper right corner.

Fig. 4.7: Close-up scanning electron micrograph of the tips of two parallel piezoresistive microlevers.

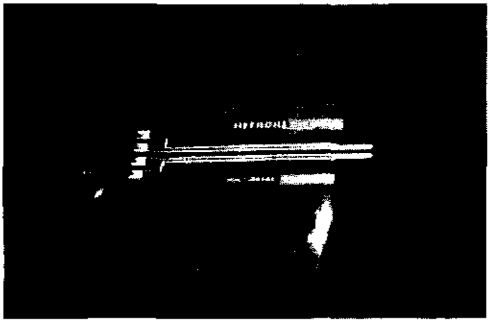

Fig. 4.8: Micrograph of a finished and assembled microlever

Table 4.3 *Corresponding values for spring constant, resonant frequency and sensitivity for typical microfabricated sensors after measuring of thickness and resistance*

ID #	t meas. [μm]	k_b theory [N/m]	f theory [kHz]	f meas. [kHz]	R meas. [kΩ]	$(\Delta R/R)_y$ [$Å^{-1}$]	$(\Delta R/R)_x$ [$Å^{-1}$]
1	2.3	20.7	320	338	4.8	- 2.3E-06	9.2E-07
2	3.1	32.4	276	298	3.1	- 2.1E-06	1.1E-06
3	3.3	5.6	59	57	2.2	-4.3E-07	1.9E-07
4	3.2	1.9	25	23	3.2	-1.7E-07	0.5E-07
5	2.9	3.3	40	40	3.1	-3.5E-07	2.5E-07

4.3 Performances of the piezoresistive cantilevers

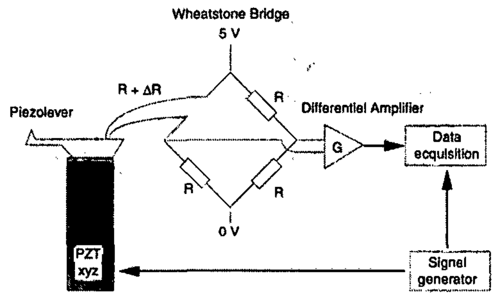

Fig. 4.9: Measurement set-up for the characterization of the piezoresistive microlever

First we characterize the devices with respect to their frequency response. We vibrate the device by means of a PZT and measure the sensor response with the set-up shown in Fig. 4.9. The output of the one element varying Wheatstone Bridge is given by

$$\Delta V = V_2 - V_1$$

$$= V\frac{\Delta R}{2(2R + \Delta R)} \qquad (4.12)$$

This bridge signal is amplified by means of a low-noise instrumentation amplifier with adjustable gain G. The amplifier output is given by $V_{out} = G\,\Delta V$.

According to the result of Table 4.3 a tip displacement of 1 nm results typically in a relative resistance change $\Delta R/R$ in the order of $\cong$ 5E-06. For a resistor of $R = 3\ k\Omega$ this represents a change of $\Delta R = 0.015\ \Omega$. The corresponding bridge output signal with a bias of $V = 5$ V is $\Delta V \cong 6\ \mu V$. After the amplification with a gain G we obtain $V_{out} = 12$ mV/nm.

It is also interesting to determine the cantilever resonant characteristics, for instance for high-speed scanning applications where the cantilever has to follow surface topography variations above 100 kHz, or for non-contact mode imaging where the cantilever is vibrated and the proximity of a surface feature is detected by shifts in the resonance frequency. In resonant applications the quality factor Q is important. We define Q as the ratio between the resonant frequency f_{res} and the frequency span Δf between the two points at the half of the maximum amplitude, i.e. $Q = f_{res} / \Delta f$. Fig. 4.10 shows a measured amplitude of a typical lever near its resonance frequency. One data has been taken in atmospheric pressure, the other in a vacuum of about 0.02 mbar. The quality factor Q of the resonance amounts to about 150 and 2000, respectively.

For our surface imaging experiments we mounted the devices in a commercial SFM instrument[9]. Fig. 4.11 shows a SFM image taken with one of our piezoresistive microlever of a calibration grating. The material is glass and the grating has a wavelength of about 1 μm. Vertical feature size is about 200 nm. Fig. 4.12 shows an image taken of an integrated circuit pattern with vertical feature size of ≅ 1 μm. Fig. 4.13 shows the topography of a micro electrode device. It consists of a pattern of Pt on Silicon/Silicon dioxide. The structure height is 150 nm. All the presented data are unfiltered.

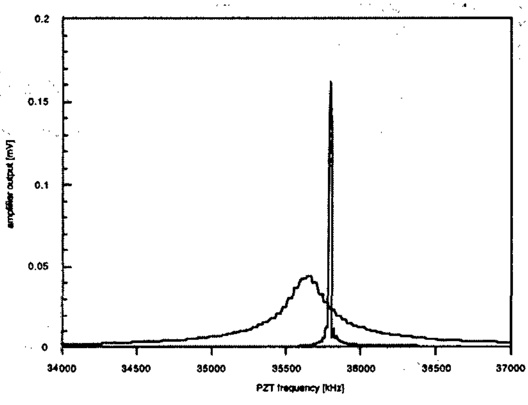

Fig. 4.10: Resonance curves of a typical piezoresistive cantilever measured with the signal of the Wheatstone bridge set-up. Quality factor at atmospheric pressure is about 150 and under vacuum about 2000.

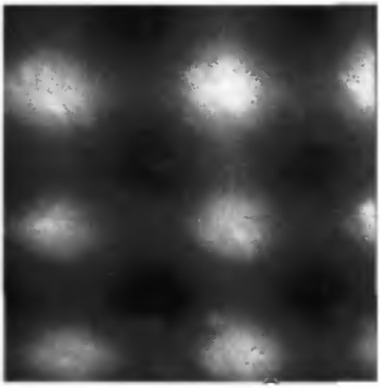

Fig. 4.11 Surface topography of a calibration grating. The material is glass. The grating wavelength is 1 µm, and the vertical modulation is about 200 nm. The scan window is 2 µm x 3 µm. Data are raw.

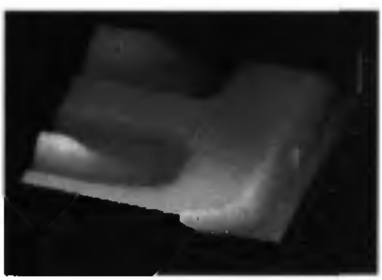

Fig. 4.12 Surface topography of a portion of an integrated circuit. The material is photoresist on metal and polysilicon. The vertical modulations about 1 µm. The scan window is 5 µm x 6 µm. Data are raw.

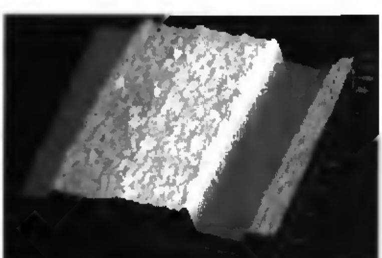

Fig. 4.13: Surface topography of a micro electrode structure. The material is Pt on Silicon/silicon nitride. The structure height is 1500 Å. The scan window is 5 µm x 7 µm. The data are raw.

4.4 Parallel imaging with an array of microlevers

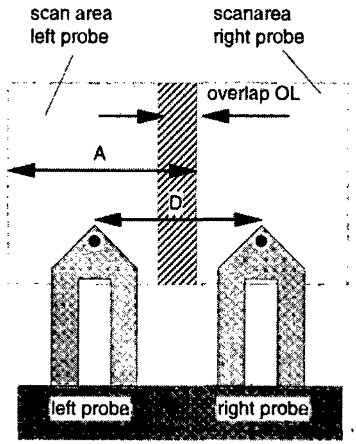

Fig. 4. 14: Simultaneous imaging of a sample surface by using two parallel piezoresistive cantilever probes. If the scan width A is larger than the tip-to-tip distance D the overlap OL allows to assemble the two images.

In order to study the feasibility of parallel imaging with a probe array we microfabricated parallel piezoresistive microlevers. For the demonstration experiment we will use a dual probe cantilever, i.e. two parallel tips. Each probe sensor is connected to its own bridge and amplifier circuit so that each channel can be adjusted individually. For the recording of the sensor signals we use two input channels of our SFM and data acquisition system. For simultaneous measurements the dual probe has to be aligned to the sample surface. This is done by approaching the sensors to the surface until the first sensor touches the surface. This can either be observed directly or via the sensor signal. Then the second sensor is brought in sample contact by a tilt and approach procedure while keeping the first at the same position. The Dual probe is thus aligned to the sample surface when both channels give approximately the same signal. This can be controlled easily by withdrawing the probes from the sample while observing their signals.

The two tips are raster scanned over the sample. The scan area A is given by the piezotube parameters and varies between (10 µm)^2 and (120 µm)^2, depending on the piezoscanner used. The distance D between two neighbor tips for this first prototype device is typically in the order of 100 µm to 200 µm (Fig. 4.14). If an overlap image of the scan area is aimed at, then A has to be at least of equal size than D. In the case when A > D, a small overlap d in the scan images of the individual tips can be obtained, which then allows to use some pattern recognition in these overlap areas for assembling a single composite surface image.

By bringing the probes closer together, while still using the current cantilever dimensions (beam width of about 20 µm) a minimum tip to tip spacing of about 50 µm might be feasible.

For the operation and surface approaching of a multiple tip array of one dimension we could use the two border tips to monitor the touch down and adjust the parallelism of the array. The tips of the two outer microlevers are higher than the tips inside the array (Fig. 4.15), a feature that allows to use those tips also for tracking purposes (e.g. in data storage applications).

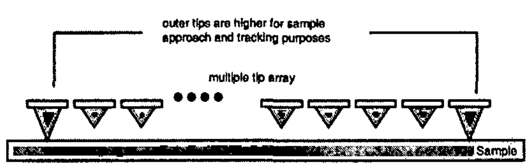

Fig. 4.15: Schematic illustration of multiprobe sample approach mechanism. The outer tips are higher and allow for a touch down monitoring.

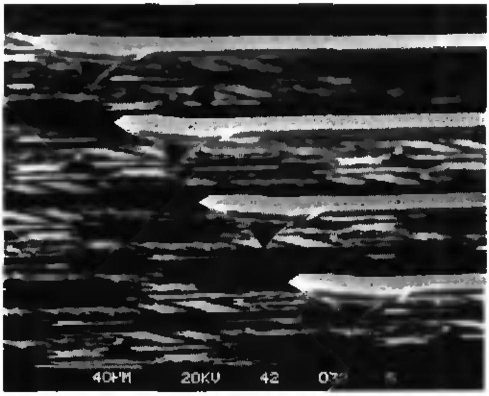

Fig. 4.16: Scanning electron micrograph of an array of silicon SFM sensors on top of the surface of an integrated circuit for parallel imaging.

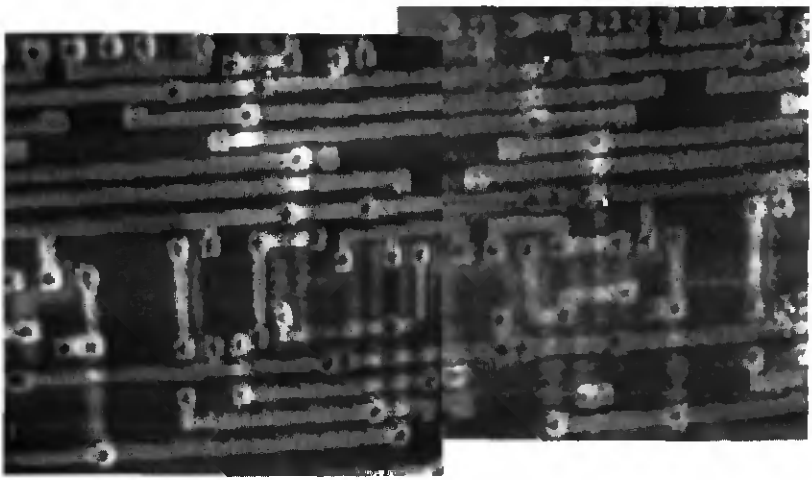

Fig. 4.17: Scan image of a portion of an integrated circuit taken simultaneously with two parallel piezoresistive cantilever probes. The tip-to-tip distance is 100 µm. The scan width is about 120 µm. The image of the left probe (a) and the right probe (b) have an overlap of about 10 µm which allows for the assembling of the total image. Data are unfiltered.

4.5 Lateral force imaging with a torsion sensor

The fabrication is identical to the normal piezoresistive cantilevers except the addition of one photolithography mask step to pattern the piezoresistors prior to the ion implantation. By this step various geometrical shapes of the resistors can be patterned. For our case we have chosen the simple shape of a single loop. Similar devices but with a different structure are currently under study by Toda and coworkers at OLYMPUS Opt. Co. [10].

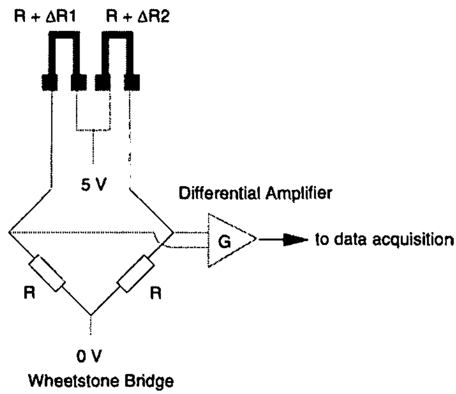

Fig. 4.18: Electronic set-up for differential measurement of piezoresistive torsion sensor. Rejection of common mode signals.

Our device dimensions are: length L = 350 μm, width = 100 μm, thickness ≅ 3 μm and tip height h = 6 μm which yields a bending spring constant k_b = 3.3 N/m and a torsional rigidity k_t ≅ 5300 N/m.

The torsion sensor can be operated in two modes. One mode is to use a configuration where the two signals are fed into the same Wheatstone Bridge for direct differential measurements and amplification (Fig. 4.18). In this case we have the advantage to reject unwanted common mode signals such as thermal drift or other noise influence. However we also reject the signal occurring from the normal bending of the cantilever. This is a drawback when a feedback control system for constant force operation is required. In a future design, it might be advantageous to integrate a third piezoresistor at the center to measure the bending independently of the torsion, which could be used for feedback purposes.

Another possibility is to use the outputs of the two piezoresistor loops individually. This means that the two signals remain separate up to the data acquisition system, where the differential signal or any other data calculation can be performed. We have operated both configurations successfully.

For the lateral force imaging we mounted the sensor in a commercial instrument[9]. We demonstrate the sensitivity to lateral forces by imaging a test grating with a step height of 15 nm (Fig. 4.19). The torsional signal (i.e. the lateral force information) is recorded during the raster scan over the steps (Fig. 4.20). We can identify the edges where the relative torsion of the cantilever increases (brighter contrast) and decreases (darker contrast) for the step-up and step-down motion, respectively. Fig. 4.21 shows the signal of one line scan across the sample. In this imaging mode no difference in contrast can be seen on top and at the bottom of the grating since it is uniform in chemical composition and no friction difference occur.

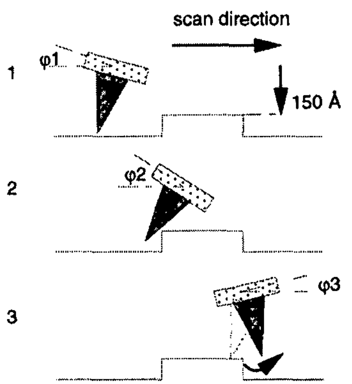

Fig. 4.19: Demonstration experiment for lateral force detection; 1) cantilever torsion φ1 due to surface friction, 2) φ2 due to geometrical edge, 3) inverted torsion φ3 at step down motion.

might be advantageous to integrate a third piezoresistor at the center to measure the bending independently of the torsion, which could be used for feedback purposes.

Another possibility is to use the outputs of the two piezoresistor loops individually. This means that the two signals remain separate up to the data acquisition system, where the differential signal or any other data calculation can be performed. We have operated both configurations successfully.

For the lateral force imaging we mounted the sensor in a commercial instrument[9]. We demonstrate the sensitivity to lateral forces by imaging a test grating with a step height of 15 nm (Fig. 4.19). The torsional signal (i.e. the lateral force information) is recorded during the raster scan over the steps (Fig. 4.20). We can identify the edges where the relative torsion of the cantilever increases (brighter contrast) and decreases (darker contrast) for the step-up and step-down motion, respectively. Fig. 4.21 shows the signal of one line scan across the sample. In this imaging mode no difference in contrast can be seen on top and at the bottom of the grating since it is uniform in chemical composition and no friction difference occur.

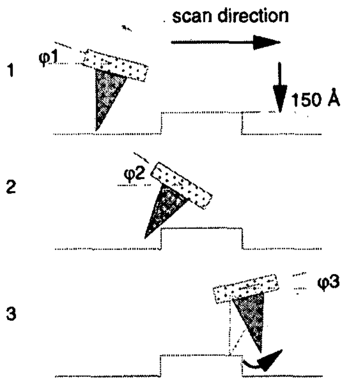

Fig. 4.19: Demonstration experiment for lateral force detection; 1) cantilever torsion φ1 due to surface friction, 2) φ2 due to geometrical edge, 3) inverted torsion φ3 at step down motion.

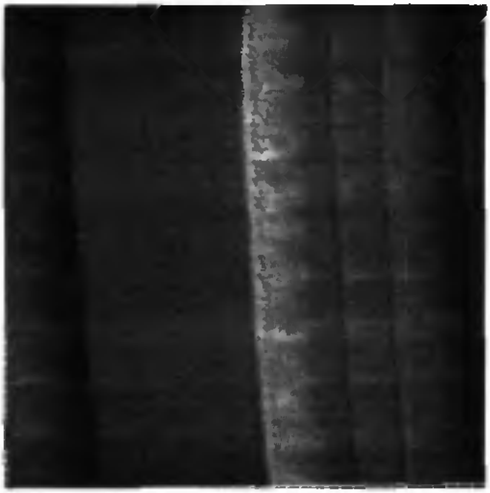

Fig. 4.20: Lateral force image of a grating. The material is structured TaO_2 on glass. Grating height is 150 Å. Only the scan in the right direction is shown. Bright contrast corresponds to higher torsion and thus to higher friction, lower contrast correspond to less torsion i.e. less friction, as it happens during the step down motion.

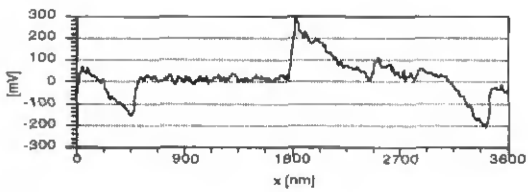

Fig. 4.21: Signal recorded during one line scan in right direction of the above image. The signal increase at the step up and the decrease at the step down is clearly visible. The amplifier gain was set to G = 2000.

4.6 Conclusions

In this chapter we have discussed a piezoresistive microlever for SFM. We have presented the analysis of the stress induced resistivity change in a doped silicon beam. By patterning the resistor loops appropriately on the stressed beam, the lever sensor becomes not only sensitive to bending, but also to lever torsion. Due to IC compatible batch fabrication techniques, we can build arrays of probes with identical properties. This can be used in parallel surface imaging with an increased scan rate, when compared to single probe operation. We have shown experimental data of SFM images, taken on rough surfaces (gratings, IC), that agree well with images taken with standard SFM systems. We have demonstrated the feasibility of multiple probe operation by imaging an IC surface with a double cantilever. Furthermore, lateral force microscopy with a piezoresistive microlever with integrated torsion sensing was performed successfully.

---

1 e.g. B. Kloeck; Dissertation University of Neuchâtel, 1989, and the references therein

2 e.g. T. Tschan, Dissertation University of Neuchâtel, 1992, and the references therein

3 M. Tortonese, H. Yamada, R.C. Barrett and C.F. Quate, Technical Digest of Transducers '91, June 24-28, 1991, San Francisco; M. Tortonese, R.C. Barrett and C.F. Quate, Appl. Phys. Lett. 61, 1993, p. 22

4 Y. Kanda; IEEE Transactions on Electron Devices, ED-29, pp. 64-70 (1982)

5 W. Pietrenko; Physica Status Solidi - Section A Applied Research 41, pp. 197-205 (1977)

6 J. Colchero, PhD. Dissertation, University of Konstanz (1993)

7 "Properties of Silicon'; emis Datareviews Series; No. 4, Inspec IEE, London 1988

8 e.g. Jaecklin, PhD thesis, University of Neuchâtel, 1993

9 Atomic Scale Tribometer™, CSEM Inc., Neuchâtel, Switzerland

10 Y. Karniya, H. Ueda, M. Takayama, Y. Nakamura, N. Sakai, K. Matsuyama, A. Toda; 55th Autumn Meeting of the Japan Society of Applied Physics September 21, 1994

1296

Chapter 5
xy-Microscanner

The scanning of a local probe over a surface requires accurate control of the position and motion of the tip. In the previous chapters, we have seen how a capacitive silicon microlever can be used as a combined sensing and actuating probe in z-direction vertical to the surface. We have also seen how a piezoresistive cantilever can be used for integrated sensing of cantilever (in z direction and in lateral direction x).

The missing block for a fully stand-alone SFM system is the integrated xy-scan mechanism. By stand-alone we mean here that the tip is moved over the sample, which is at rest. This provides more flexibility in operation. A microfabricated scanning unit would be of great benefit because it does not need any assembling of hybrid elements, and, in addition, its immunity to thermal and vibrational noise decreases with compactness and miniaturization.

Akamine and co-workers[1] followed this concept with a microfabricated tunneling microscope that incorporates piezoelectric actuators capable of three dimensional motion for the scanning of the tip and the control of the tip-sample tunneling gap. The use of piezoelectric materials however makes it difficult to integrate a protruding tip. Hence with their design only flat layered materials could be imaged successfully.

Another technique suitable for building micro-actuators is the so-called sacrificial layer technology. It has recently gathered much interest as a potential method of constructing micromechanical elements for scanned probes[2,3]. The devices based on this technology are driven electrostatically; especially the comb actuator proves to be a useful driving unit [4]. Its main characteristics are a quick response time, IC compatible driving voltages, no hysteresis in the positioning and no creep. Furthermore, it should be feasible to integrate capacitive or piezoresistive displacement monitoring. These features make the comb actuator an interesting candidate for the actuation of an SFM tip.

Jaecklin and co-workers at the IMT have successfully developed polysilicon micro actuators based on this principles[5]. This chapter shows briefly recent advances that we have obtained for a micromechanical xy-scanner with tip and introduces the first prototypes and preliminary experimental results of such an integrated tip raster scan mechanism for SFM.

5.1 Design of an electro-static xy-scanning device

In order to obtain a planar xy scanning device based on the electrostatic actuation principle, it is suitable to arrange four comb drives around a center stage as shown in the schematic Fig. 5.1. Typical dimensions of the device that we constructed are a total beam length of $L = 600\ \mu m$, a beam width of $w = 2\ \mu m$ and a beam thickness of $t = 4\ \mu m$.

The comb drive itself consists of two electrodes: the fixed electrode and the movable electrode. The functional components of the latter are the suspension beams, which provide a mechanical guidance for the actuator motion, and the comb, where the force for the actuation is generated. A schematic overview is given in Fig. 5.2. The design of the micro stage is based on a pull mechanism, i.e. the table with the tip is moved to any position in the xy-plane by activating two of the four comb drives. With our device dimensions and with a typical comb suspension length of $l = 200\ \mu m$ and a finger gap $g = 2\ \mu m$, we can calculate the displacement of the tip on the center stage on the beam cross via the force created in the combs. This force can be expressed by[5]

$$F_C = \frac{nh\varepsilon V^2}{g}$$

where n is the number of the comb fingers ($n = 16$ in our case). For the typical beam height $h = 4\ \mu m$ and for a DC voltage of 30 V we obtain a pulling force of 0.25 μN per comb actuator.

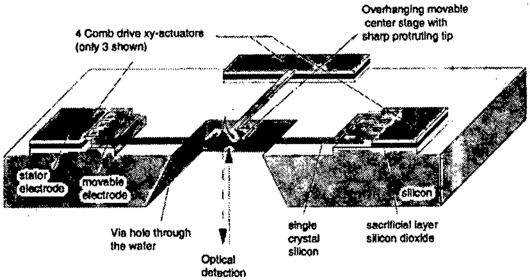

Fig. 5.1 Schematic representation of the planar xy-microscanner with tip for SFM applications, with via hole for optical monitoring. For the operation principle and dimensions please refer to the text.

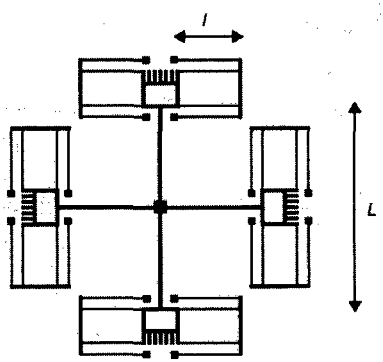

Fig. 5.2 Overview of the beam arrangement including the xy-table and the suspensions. Typical dimensions are L = 600 μm and l = 200 μm.

The lateral displacement Δx (or Δy) due to this force can be expressed via the force constants in that direction by using Hook's law, i.e. $\Delta x = F/k_x$, where k_x is the effective total spring constant in x direction. k_x is composed of the lateral force constants k_{xb} of the beam and by k_{xs} of the comb suspensions. We will make the simplifying assumption that the two ends of the crossed beams are fixed. Then, the two components can be expressed by

$$k_{xb} = \frac{16Ew^3h}{L^3} \qquad \text{and} \qquad k_{xs} = \frac{2Ew^3h}{l^3}$$

where l denotes the length of the suspension beams (in our case l = 200 μm). The total lateral stiffness is the sum of the force constants, i.e. the two suspensions (the pulling comb plus the opposite inactive comb) plus one cross beam. Thus, the total lateral stiffness becomes

$$k_x = 2k_{xs} + k_{xb}$$

For a typical device we evaluated following values: $k_{xb} = 0.4$ N/m, $k_{xs} = 1.35$ N/m, and $k_x = 3.1$ N/m. For this device the lateral displacement for a driving voltage of 30 V is 80 nm in one direction. When addressing all four comb actuators in the way to add up the partial scan areas, then the tip on the center stage can be scanned in a square of 160 nm x 160 nm = 25'600 nm^2. By applying voltages in the range of 100 to 300 V a displacement of several μm can be achieved. The decoupling of the z- and y-position is given by the construction of the suspension and is optimized for this device. Fig. 5.3 shows an illustration of how the tip covers the scan area. By driving the 4 combs in a suitable way the full scan range can be achieved. A typical curve that shows the tip lateral displacement as a function of the applied voltage on the driving comb fingers is shown in Fig. 5.4.

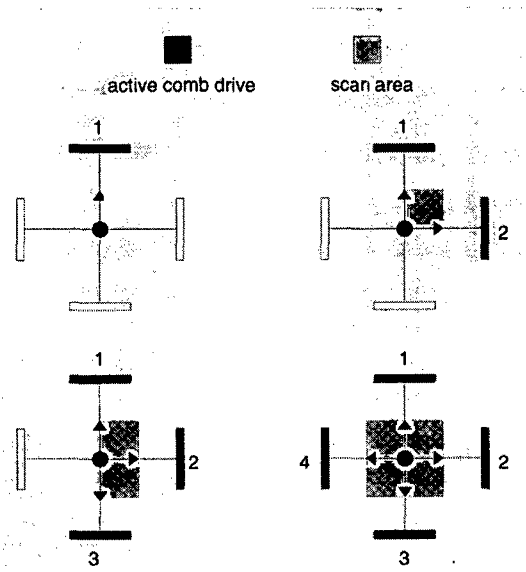

Fig. 5.3: Principle of 4-comb operation to achieve full scan range of the xy-table.

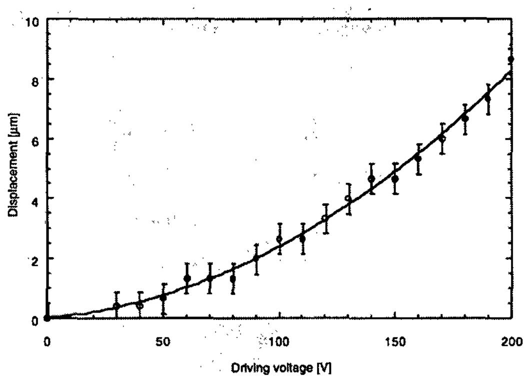

Fig. 5.4: Typical displacement curve for a micromachined xy-scanner as a function of the applied voltage[6]*.*

The vertical force constant k_Z can be calculated in a similar way. Again we assume double sided clamped beams. With the additional approximation that the force constant of 2 crossed beams of width w is the same as the force constant of 1 beam of width w' = 2w, then the vertical force constant becomes

$$k_Z = \frac{16Eh^3w'}{L^3}.$$

Using our typical dimensions we get $k_Z = 3.2$ N/m. A typical force F_Z during SFM scanning lies in the order of 1 nN and thus displaces the center stage by about $\Delta z = 0.3$ nm which can be measured by means of optical detection methods (beam deflection or interferometer).

For high speed scanning applications and for good immunity against vibration noise the resonance frequency of the table should also be high, possibly above a few tens of kHz. The first resonance frequency of the cross for free vibrations in z direction can be calculated by

$$f = \frac{1.03}{L^2}\sqrt{\frac{Eh^2}{\rho}}$$

where $\rho = 2300$ kg/m^3 is the density of silicon. For the typical dimensions f is in the order of 100 kHz.

A further key feature of our device is the via hole that has been etched through the wafer leaving the micro stage with the tip overhanging the substrate rim. This enables the monitoring of the tip-sample interaction and optical measurement of the vertical displacement of the scanned probe.

5.2 Microfabrication: from poly- to mono-crystal silicon

Jaecklin and coworkers at the IMT have operated comb actuators made of *poly-crystalline silicon* fabricated by means of surface micromachining and sacrificial layer etching techniques. The deposited thin film (Å 2-3 µm) of structural layer is not well suited for the fabrication of sharp protruding tips, as we described in chapter 2. Therefore we developed a process for a scan device by using *single-crystalline silicon* as material.

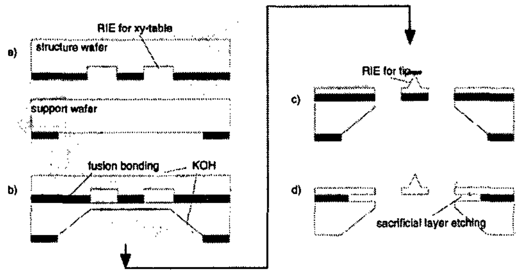

Fig. 5.5: Fabrication steps for the micromachining of the silicon xy-scanner; a) two wafers are needed, the top wafer is structured with RIE to the structural shape of the xy-table, b) aligned silicon fusion bonding and KOH membrane etching, c) RIE for tip, d) sacrificial layer etching to release movable parts.

The process is almost identical to the process to fabricated the capacitive micro levers described in chapter 3. In the basic version the process requires a set of three masks. The fabrication steps are illustrated in Fig. 5.5. After thermal oxidation (1.5 μm) and patterning of two silicon wafers, 3 μm deep structures are formed by reactive ion etching (C_2ClF_5/SF_6 plasma) in the upper wafer to define the shape of the xy-actuator (a). Precision alignment and pre-bonding on a commercial mask aligner is followed by thermal annealing (1100_C, 3 h) and fusion bonding of the wafers on their SiO_2-SiO_2 contact areas (b). Via hole etching of the lower wafer and simultaneous thinning of the upper wafer are performed in KOH until an about 10 μm thick membrane remains (b). Deposition and patterning of a tip mask on the top surface is followed by dry and wet etching to produce the probe tips on the xy-stage (c). In the last step the sacrificial silicon dioxide layer is laterally etched in BHF which releases the beams (d). Fig. 5.5 shows a SEM micrograph showing the center portion of the microfabricated xy-table after sacrificial oxide layer etching. The table is freestanding and supported by the crossed beams.

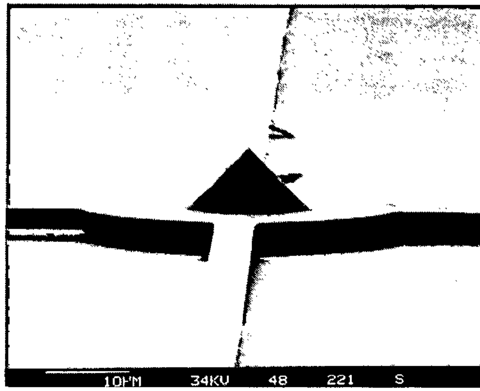

Fig. 5.6: SEM image of the tip on the center stage, without via hole. It can be nicely seen that the profile of the tip (pyramidal) and the beams (vertical) are possible by the aligned wafer bonding technique due to the separation of incompatible process steps on different sides of the substrate.

5.3 Experimental results and suggested improvements

Recently, Indermühle and coworkers have successfully fabricated and operated an improved device with via hole. For a voltage of 300 V, a displacement of 12 µm could be observed. The measured resonance frequencies in the first vertical and lateral mode are above 10 kHz.

The tip was approached to a sample (tungsten needle) and raster scanned across it by means of the comb drive actuators. The motion of the table was monitored with an optical fiber interferometer. The vertical displacement of the stage during the scanning was measured. The image of the surface topography of the sample obtained by the microscanner is in good agreement with the image taken by a conventional instrument.

Thus an autonomous xy tip scan mechanism by using micromechanical elements is demonstrated. Unfortunately the planar xy-scanner has the inherent drawback of poor tip accessibility. So far only convex samples could be imaged. Improvements as suggested by Indermuehle are for instance to use backside electrode contacts to improve tip clearance.

It is a promising tool for implementation in true stand-alone SFM systems, where the tip is raster scanned, and not the sample, without using the bulky PZT scanners. A further advance would be to operate several xy-scanners in parallel for particular applications, such as IC inspection or data storage.

---

[1] S. Akamine, T.R. Albrecht, M.F. Zdeblick and C.F. Quate, Sensors and Actuators A, 21-23, 1990, p. 964

[2] D. Kobayashi, T.Hirano, T. Juruhata, H. Fujita; Digest MEMS Workshop, Travemünde, Germany, 1992, p. 214

[3] J.J. Yao, S.C. Arney, N.C. MacDonald; J. Microelectromech. Syst. 1, p. 147

[4] C.J. Kim, A.P. Pisano, R.S. Muller and M.G. Lim, Tech. Dig. IEEE Solid-State Sensor and Actuator Workshop, Hilton Head Island, SC, June 4-7, 1990, p.48

[5] V.P. Jaecklin, PhD. dissertation, University of Neuchâtel, 1994

[6] P.F. Indermühle, C. Linder, J. Brugger, V.P. Jaecklin and N.F. de Rooij

1296

Final Conclusions

In my Ph.D. thesis I have presented the results that we obtained in the field of silicon microfabrication of sensor and actuator devices for the scanning force microscope. The fabrication techniques were presented for building cantilevers with sharp tips, that were then successfully used for imaging in SFM systems. We have seen that for the various applications, different tip characteristics such as shape and sharpness are needed. For obtaining ultra-sharp tips with a radius in the range of 1 nm, a low temperature oxidation sharpening was successfully performed.

We have also seen the integration of a variety of functions into the cantilever probe, such as deflection sensors (capacitive and piezoresistive) and an actuation mechanism (electrostatic). These features are mandatory if the operation of tip areas for parallel probing is aimed at. The analysis of the capacitive sensor and actuator has shown that the device is best operated in a dynamic mode, that is, by vibrating the cantilever in resonance by means of the electrostatic forces in the capacitor. When the tip 'feels' a surface force gradient, the beams resonant frequency shifts slightly, which is hence a measure of surface topography. By using this mode the tip is dithering like in a 'tapping' mode over the surface. To our knowledge, this is the first operation of such a device using a built-in electrostatic actuator, fabricated by silicon technology. The proposed device is well suited for parallel tip operation, which, however has yet to be demonstrated.

Parallel imaging has been presented by using two piezoresistive cantilevers placed side by side with a tip-to-tip distance of 100 micrometers. A parallel bridge set-up has been used to measure the signals. When parallel probing using a, say, 1000 fold cantilever area is aimed at, a new signal pick-up scheme has to be implemented by using multiplexing, for instance. Another problem in parallel operation of cantilevers may arise from the necessary adjustment or the individual fly height of each probe over the sample. Prospective integrated actuators include electrostatic forces and piezoelectric films. Further process development has to be done to combine actuator and sensor function into one device.

I have also presented a particular version of a piezoresistive SFM sensor to measure the torsion of the cantilever in a tribological experiment. Such an integrated lateral force sensor is much smaller than the conventional 4 segment photodetector, thus following the same miniaturization trend as for normal deflection sensors and enabling multiprobe operation.

In summary, we have shown various microfabrication processes for building SFM sensors and their operation. We have found, that for each specific surface scanning application a particular tip-cantilever characteristic is required. With other words, there is probably not a unique local probe that can fulfill simultaneously all the possible requirements. The optical beam deflection technique, e.g., is a set-up that is relatively simple, reliable and easy to use. For most standard SFM applications it will for long time be the dominant detection principle.

However, for particular applications, and especially when the available space for the probe is limited (e.g. in parallel tip operation, or in adverse environment such as vacuum chambers or at low temperature), the integration of the sensing and actuation functions into the probe itself is necessary. Microfabrication techniques are an important way to meet these goals, allowing simultaneously for the cost-effective batch-fabrication of large amounts of SFM devices on a silicon wafer.

Publication list

Parts of the work presented in this thesis have contributed to the following publications:

R.A. Buser, J. Brugger, N.F. de Rooij
"Micromachined Silicon Cantilevers and Tips for Scanning Probe Microscopy"
Ultramicroscopy, No 42-44, North Holland, pp. 1476-1480, 1992
Microelectronic Engineering, Vol. 15, pp. 407-410, 1991

J. Brugger, R.A. Buser, N.F. de Rooij
"Silicon Cantilevers and Tips for Scanning Force Microscopy"
Sensors & Actuators A, 34, pp. 193-200, 1992

J. Brugger, R.A. Buser, N.F. de Rooij
"Micromachined atomic force microprobe with integrated capacitive read-out"
J. Micromech. Microeng., 2, pp. 218-220, 1992

J. Brugger, V.P. Jaecklin, R.A. Buser, C. Linder, N.F. de Rooij
"Micromachined Silicon Tools for Nanometer-Scale Science"
NATO - ARW: Manipulation of Atoms under High Fields and Temperatures: Application, Lyon, France, July 6-10, 1992; Nanosources and Manipulation of Atoms Under High Fields and Temperatures: Applications, V.T. Binh et al. (eds.), pp. 311-317, Kluwer Academic Publishers 1993

J. Brugger, R.A. Buser, N.F. de Rooij
"High-precision aligned silicon wafer bonding for a micromachined AFM sensor"
Proceedings Volume 93-29, M.T. Schmidt et al. (edts.) pp. 363-372; The Electrochemical Society, Inc., ISBN 1-56677-068-8

J. Brugger, N. Blanc, Ph. Renaud and N.F. de Rooij
"Microlever with combined integrated sensor/actuator functions for scanning force microscopy"
Sensors and Actuators Vol. 43, No. 1-3, pp. 339-345

V.P. Jaecklin, C. Linder, J. Brugger, N.F. de Rooij and J.-M. Moret, R. Vuilleumier
"Mechanical and optical properties of surface micromachined torsional mirrors in silicon, polysilicon and aluminum"; Sensors and Actuators A, 43 (1994) 269-275

P.F. Indermuehle, J. Brugger, V.P. Jaecklin, C. Linder, N.F. de Rooij
"Design and Fabrication of an Overhanging XY-Microactuator with Integrated Tip for Scanned Surface Profiling"
to be published in: Sensors and Actuators

J. Brugger, V.P Jaecklin, P.F. Indermühle, C. Linder
"Microsystems Research and Development at IMT Neuchâtel - Scanning Probe Microsystem for Nanotechnology"
Micro Machine, Journal of Micromachine Society, Vol. 6, No 1, ISSN 0917-0103, p. 105, April 1993

J. Brugger, P.F. Indermühle, V.P Jaecklin, C. Linder, N.F. de Rooij
"Nanopositioniersystem"
in Mikromaschinen, Fachbeilage Mikrosystemtechnik, Publication of VDI/VDE-Technologiezentrum Informationstechnik, me Bd. 7 (1993) Heft 5, p. 78

J. Brugger
"Silicon micromachines"
NESTLING TIMES, No. 2, Sept. 1993, The newsletter of the Network of European Scientists and Technologists in Japan (NEST)

J. Brugger, V.P. Jaecklin, C. Linder, N. Blanc, P.F. Indermuehle, N.F. de Rooij
"Microfabricated Tools for Nanoscience"
J. Micromech. Microeng., 2, pp. 1-8, (1993)

J. Brugger, J. Burger, M. Binggeli, R. Imura and N.F. de Rooij
"Lateral force measurements in a scanning force microscope with piezoresistive sensors"
Digest of technical papers, pp. 636-639, Transducers '95, Stockholm, Sweden, June 25-29, 1995

N. Blanc, J. Brugger, N.F. de Rooij, U. Dürig
"Scanning Force Microscopy in the dynamic mode using microfabricated capacitive sensors"
to be published in J. Vac. Sci. and Technol. B, March/April 1996

Unpublished

J. Brugger
"Studies on microstructures for the application in the atomic force microscope"
Diploma, Faculty of Science, University of Neuchâtel, Switzerland, 1990

J. Brugger
"Microfabricated sensor array for ultra-high density point recording information storage system"; Hivips report 306G, HITACHI Advanced Research Laboratory, Tokyo, Japan (1994)

Patent:

R. Buser, J. Brugger, C. Linder (Appls. & Invs.), British Technology Group Ltd. (Appl.), Microprobe for Surface-Scanning Microscopes, Patent, PCT/GB92/01060, 12 June 1992

Curriculum vitae

Name:	Jürgen Brugger	
Birth:	11. November 1963 in Säckingen, Germany as son of Peter and Charlotte Brugger, born Bernauer	
Education:	1970-1983:	'Grundschule' and 'Gymnasium' in Rheinfelden/Germany
	1984-1990:	Studies at the University of Neuchâtel, Switzerland Degree in "Electronique Physique"
	1991-1995:	Dissertation at the IMT, University of Neuchâtel "Microfabricated tools for the Scanning Force Microscope" Microfabricated Sensors, Actuators and Microsystems Group

Industrial projects:

EM Microelectronic-Marin S.A.

1985-1988:	Wafer processing in CMOS fabrication line
1988:	Development of 3 μm HCMOS and 'Bumping' technology
1989:	Creation of an IC-Development Book
1993-1994:	Visiting research position at the 'Advanced Research Laboratory', HITACHI Ltd., in Kokubunji-shi, Tokyo, Japan

Teaching Activities:

1990-1995 :	Teaching assistant at the IMT, University of Neuchâtel, Switzerland

I owe my university education to following lecturers of the University of Neuchâtel:

J.P. Amiet, Y. Baer, M. Banderet, H. Beck, M. Bourgeois, H. Buczek, N.C. Bui, R. Dändliker, M. Degrauwe, Y. Dodge, M. Erard, R. Guye, H. Hügli, P. Huguenin, E. Jeannet, P. Martinoli, W. Marty, F. Pellandini, C. Piquet, N.F. de Rooij, A. Robert, A. Shah, W. Sörensen, U. Suter, J. Vuilleumier, J. Weber

NANOMETER SCALE MESSAGE IN GOLD

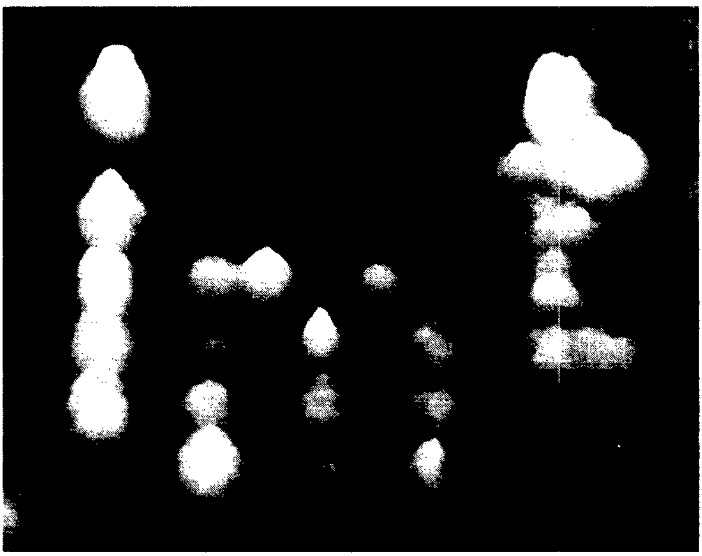

Scanning Force Microscope image of gold dots with ≅ 30-50 nm diameter. Image size:≅ 1x1.2 micron. The dots have been formed by field evaporation of gold from the tip of the same SFM cantilever as used to form this image. Image courtesy of Mr. Koyanagi, Hitachi Adv. Res. Lab., presented by Asai-san and Imura-san during their visit at the IMT Neuchâtel on September 23, 1994.